Journal of Zhejiang University-SCIENCE A (Applied Physics & Engineering) 2022 23(7):505-526
www.jzus.zju.edu.cn; www.springer.com/journal/11582
E-mail: jzus_a@zju.edu.cn

Review

https://doi.org/10.1631/jzus.A2100627

Review of elemental mercury (Hg^0) removal by CuO-based materials

Dong YE[1]✉, Xiao-xiang WANG[2], Run-xian WANG[1], Xin LIU[1], Hui LIU[1], Hai-ning WANG[1]✉

[1]*College of Quality & Safety Engineering, China Jiliang University, Hangzhou 310018, China*
[2]*Key Laboratory of Biomass Chemical Engineering of Ministry of Education, Institute of Industrial Ecology and Environment, College of Chemical and Biological Engineering, Zhejiang University, Hangzhou 310027, China*

Abstract: Mercury emission has become a great environmental concern because of its high toxicity, bioaccumulation, and persistence. Adsorption is an effective method to remove Hg^0 from coal-fired flue gas, with adsorbents playing a dominant role. Extensive investigations have been conducted on the use of CuO-based materials for Hg^0 removal, and some fruitful results have been obtained. In this review, we summarize advances in the application of CuO-based materials for Hg^0 capture. Firstly, the fundamentals of CuO, including its crystal information and synthesis methods, are introduced. Then, the Hg^0 removal capability of some typical CuO-based adsorbents is discussed. Considering that coal-fired flue gas also contains a certain amount of NO, SO_2, H_2O, NH_3, and HCl, the impacts of these species on adsorbent Hg^0 removal efficiency are summarized next. By generalizing the mechanisms dominating the Hg^0 removal process, the rate-determining step and the key intermediates can be discovered. Apart from Hg^0, some other air pollutants, such as CO, NO_x, and volatile organic compounds (VOCs), account for a certain portion of flue gas. In view of their similar abatement mechanisms, simultaneous removal of Hg^0 and other air pollutants has become a hot topic in the environmental field. Considering the Hg^0 re-emission phenomena in wet flue gas desulfurization (WFGD), mercury capture performance under different conditions in this device is discussed. Finally, we conclude that new adsorbents suitable for long-term operation in coal-fired flue gas should be developed to realize the effective reduction of mercury emissions.

Key words: Hg^0 capture capability; CuO-based materials; Hg^0 removal mechanisms; Gas components; Simultaneous removal of multiple pollutants

1 Introduction

As a global pollutant, mercury has drawn considerable concern in recent decades owing to its bioaccumulation, persistence, and high toxicity to human beings and ecosystems (Yang et al., 2019b; Zheng et al., 2021). Coal-fired power plants are responsible for about 30% of the mercury produced, and are well recognized as the major source of mercury emissions in China (Ye et al., 2021). In view of this serious problem, a standard GB13223-2011 was issued to reduce mercury emissions to less than 0.03 μg/m^3 (Yang et al., 2019a). To meet this tough standard, it is essential to adopt effective mercury abatement techniques.

✉ Dong YE, Richard32@126.com
Hai-ning WANG, whnfyy@163.com
Dong YE, https://orcid.org/0000-0001-8299-224X
Hai-ning WANG, https://orcid.org/0000-0003-4653-0819

Received Dec. 10, 2021; Revision accepted Jan. 27, 2022; Crosschecked May 27, 2022

In general, the emitted mercury species can be classified into three main categories: elemental mercury (Hg^0), oxidized mercury (Hg^{2+}), and particulate-bonded mercury (Hg^p) (Mei et al., 2020; Ma et al., 2021). The high solubility of Hg^{2+} ensures its sufficient absorption by wet flue gas desulfurization (WFGD) devices, and Hg^p can be effectively captured by dust removal systems because of its strong adherence to particulate surfaces (Wen et al., 2011; Jampaiah et al., 2019). However, low solubility and high volatility make Hg^0 difficult to remove by existing air pollutant abatement devices, and constitutes the main barrier to the reduction of mercury emissions (Liu H et al., 2020).

Among the various air pollutant abatement techniques, injecting adsorbents into the flue gas is attracting increasing attention because it avoids the need to install additional air pollutant control devices. Generally, this process takes place in the upstream part of dust removal systems, in which the spent adsorbents can be separated from the flue gas (Mei et al., 2019). In this technology, the activity of the adsorbents plays

a crucial role in the Hg^0 removal efficiency of the whole system (Wang C et al., 2020). Some materials, such as carbon (Liu DJ et al., 2020), calcium compounds (Zhang et al., 2016; Balasundaram and Sharma, 2018), and fly ashes (Liu Z et al., 2020), are proven to be capable of capturing Hg^0 in the flue gas. Owing to its wide availability, activated carbon is used commercially for Hg^0 capture in power stations. However, the narrow operating temperature window, adverse effects on fly ash products, and high cost constrain the further practical application of carbon-based materials (Ye et al., 2021). Similarly, despite the merits of availability, the relatively poor Hg^0 capture capability and stability of Ca- and fly ash-based adsorbents have driven researchers to develop alternative materials (Liu Z et al., 2020). Metal oxide is expected to become a potential Hg^0 adsorbent material due to its merits of abundant natural reserves, wide operation operating temperature window, acceptable thermal stability, and ease of synthesis. When coupled with some other materials, an excellent Hg^0 capture performance can be obtained within a certain temperature range (Ye et al., 2021).

CuO, a typical transition metal oxide, has some attractive physicochemical properties, such as tunable textural structures, abundant surface vacancies and reactive chemisorbed/lattice oxygen, and Lewis acidity, which make it suitable for Hg^0 removal reactions (Fang and Guo, 2018). If diverse strategies, including chemical modification and substitution, are exploited, the functionalities of CuO could be improved (Chen et al., 2018; Yang et al., 2019c). Compared with carbon-, Ca-, and fly ash-based materials, CuO-based adsorbents are superior because of their wide operating temperature window, excellent stability, and satisfactory anti-poisoning ability (Fan et al., 2012; Chen et al., 2018; Galloway et al., 2018). Given these promising attributes, there has been a recent boom in research exploring the use of CuO-containing materials for Hg^0 capture at lab-scale. Many papers concerning aspects of Hg^0 adsorption performance, mechanisms, and simultaneous removal of Hg^0 with other air pollutants have been published. The results demonstrate that CuO-based adsorbents have good prospects as potential adsorbents for the abatement of Hg^0 in power plants. For these reasons, it is appropriate to review the advances in capturing Hg^0 from coal-fired flue gas using CuO-based materials. Such knowledge could provide a guideline for effectively reducing mercury emissions.

In this review, we cover progress in research on CuO-based materials for Hg^0 removal. First, the fundamentals of CuO, including crystal information and corresponding synthesis methods, are introduced. Based on the roles CuO plays in Hg^0 removal reactions, CuO-based materials can be divided into two categories, namely supported CuO adsorbents and CuO mixed oxide adsorbents. The performance of these two types of materials is illustrated next. Considering that there is a certain amount of NO, SO_2, H_2O, NH_3, and HCl in real coal-fired flue gas, the impacts of these gas species on adsorbent Hg^0 removal efficiency are summarized in Section 4. By generalizing the mechanisms dominating Hg^0 removal reactions, the rate-determining step and key intermediates can be discovered. Aside from Hg^0, some other air pollutants, such as carbon monoxide, NO_x, and volatile organic compounds (VOCs), also account for a certain portion of emissions. In view of their similar abatement mechanisms, simultaneous removal of Hg^0 with other air pollutants has become a hot topic in the environmental field, and is introduced in Section 6. After flue gas enters the WFGD, re-emission of Hg^0 always occurs, which is detrimental to the effective reduction of mercury emissions. Thus, Hg^{2+} absorption performance under different conditions in this device is introduced in Section 7. Finally, we conclude that new adsorbents suitable for long-term operation in real coal-fired flue gas should be developed to realize the effective reduction of mercury emissions.

2 Fundamentals of CuO

2.1 Crystal information of CuO

CuO is a black metal oxide with a monoclinic structure (space group, *C*2/c). Each unit cell consists of four formula units (Fig. 1). The Cu^{2+} cations and O^{2-} anions are located at the centers of inversion symmetry in a single fourfold site 4c (1/4, 1/4, 0) and site 4e (0, 0.416(2), 1/4) (Poizot et al., 2003). Lattice constants of CuO are presented in Table 1. No phase transition occurs when the pressure and temperature are lower than 70 MPa and 3000 K, respectively (Bourne et al., 1989). That is to say, in many cases CuO exhibits only a monoclinic phase, as confirmed by

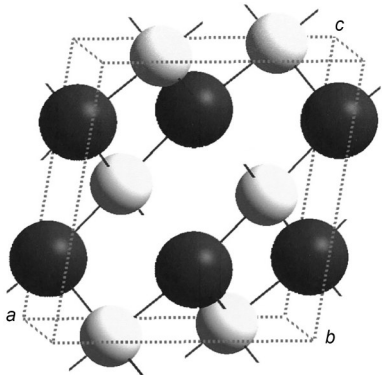

Fig. 1 Model of a CuO unit; white and black spheres represent O and Cu atoms, respectively. Reprinted from (Poizot et al., 2003), Copyright 2003, with permission from IOP Publishing, Ltd.

Table 1 Lattice constants of CuO (Poizot et al., 2003)

Lattice constant	Value
Space group	*C*2/c
Lattice constant *a* (nm)	0.4685 (0)
Lattice constant *b* (nm)	0.3430 (3)
Lattice constant *c* (nm)	0.5139 (3)
Lattice constant β (°)	99.08 (6)

Radhakrishnan et al. (2014). Although CuO has a relatively high thermal stability, researchers have discovered that the particle size and lattice parameters of CuO continuously increase as the calcination temperature is elevated (Vidyasagar et al., 2012).

2.2 Preparation of CuO

Because CuO with other crystal structures, such as cubic and tetragonal phases, are rarely seen in catalysis and adsorption reactions, in this section we introduce the methods of synthesis of monoclinic CuO, the most common phase under normal conditions. It is well-recognized that mainly solution-based, solid-state, and electrochemical methods are adopted to prepare CuO materials.

2.2.1 Solution-based methods

A relatively low reaction temperature and pressure, together with a controllable morphology, composition and production, have led to increased attention on solution-based methods. Among the various solution-based methods, hydrothermal/solvothermal, precipitation techniques are proven to be capable of synthesizing the target materials.

The preparation of CuO nanoparticles, also called 0D CuO materials, can be divided into two steps. First, cupric precursor reacts with a base solution, including ammonium hydroxide, NaOH and Na_2CO_3, to form $Cu(OH)_2$. Then, the produced $Cu(OH)_2$ is dehydrated at certain temperatures to obtain the final CuO product. Based on this concept, Neupane et al. (2009) and Chakraborty et al. (2011) used the inorganic precursor, $Cu(NO_3)_2$, and the organic precursor, copper acetylacetonate, to successfully synthesize CuO nanoparticles with a size of several nanometers. For the synthesis of 1D, 2D, and 3D CuO materials, in addition to a copper precursor and a precipitation agent, a surfactant/capping agent is involved. There are two different opinions regarding the mechanism of formation of CuO nanostructures with the use of a surfactant. The first proposes that the surfactant/capping agent is selectively adsorbed on certain facets of monoclinic CuO crystals, which then kinetically control the growth of the facets and hence the orientation of the crystals. The second proposes that the added surfactant/capping agent acts as a template for the formation of CuO materials with various morphologies. Besides, OH^- anions somehow influence the number of nuclei and the concentrations of growth units of the CuO crystals in reaction systems, which consequently determine the dimensions and morphologies of the final products. Li et al. (2010) used PEG (polyethylene glycol) 200 as the capping agent to prepare CuO nanowires with an aspect ratio of several hundred. Given that PEG was present and the ratio of OH^-/Cu^{2+} exceeded 4, ultra long CuO nanowires could be obtained. Otherwise, only CuO nanoleaves growing along the [111] direction were formed, confirming that the surfactant/capping agent and OH^- were essential for the formation of CuO nanowires. Similarly, Yang et al. (2013) used $CuSO_4$ as the copper precursor, PEG as the surfactant, NaOH and urea as the precipitants to prepare CuO materials with different morphologies (Fig. 2). As the amount of PEG and $CuSO_4$, and the temperature in the precipitation stage were adjusted, the resulting CuO was transformed from a particle-shaped product to sheet- and rod-shaped products. This is because apart from the effect of the surfactant, ammonia coming from the decomposition of urea can facilitate the dissolution of CuO to a certain extent, and in turn have some impact on the recrystallization of CuO. This consequently contributes

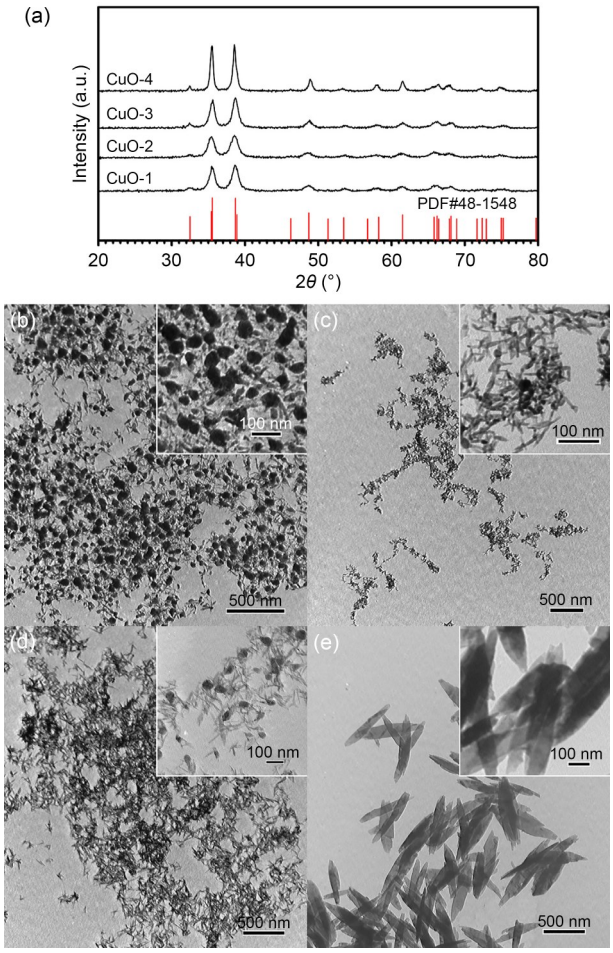

Fig. 2 X-ray diffraction (XRD) patterns (a) and transmission electron microscope (TEM) images (b)–(e) of CuO particles with different shapes. Reprinted from (Yang et al., 2013), Copyright 2013, with permission from Elsevier

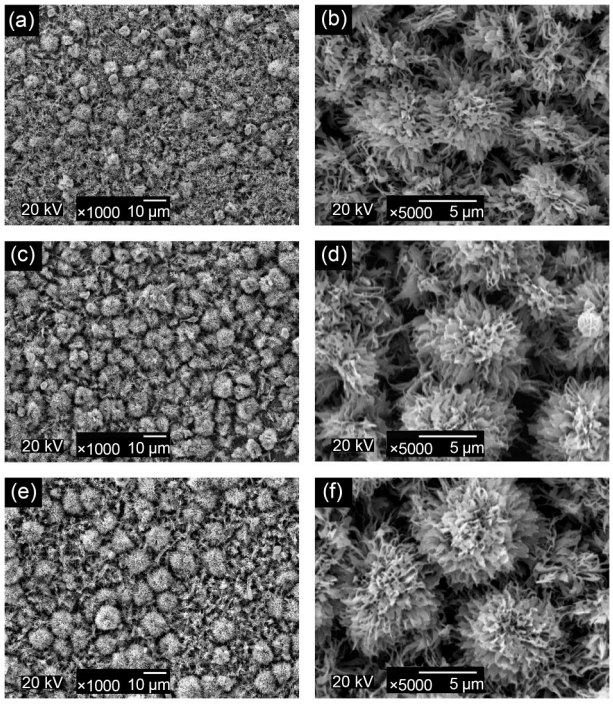

Fig. 3 Scanning electron microscope (SEM) images of CuO nanostructures prepared after 25 min ((a) and (b)), 25 min ((c) and (d)), and 40 min ((e) and (f)). Reprinted from (Zhang et al., 2008), Copyright 2008, with permission from AIP Publishing

to the various dimensions and morphologies of the final products.

Generally, most cases related to the solution-based synthesis of CuO materials are based on solutions containing Cu^{2+} salt. But sometimes metallic Cu substrates have been used as the copper precursor to prepare CuO in the presence of some oxidative agents, such as $(NH_4)_2S_2O_8$ and $K_2S_2O_8$. Zhang et al. (2008) fabricated CuO nanoflowers on Cu substrates using $K_2S_2O_8$ as the oxidant under basic conditions at 70 °C. When the reaction lasted for 15 min, materials with grass-like and flower-like structures coexisted. When the reaction process was ongoing, the relative concentration and size of nanoflowers increased. By extending the reaction time to 40 min, nanoflowers of 8–11 μm were obtained (Fig. 3). It was claimed that Ostwald ripening could explain this morphology evolution process. Similarly, Liu et al. (2006) demonstrated fabrication of CuO nanostructures on Cu substrates using O_2 as the oxidative agent in ammonia- and NaOH-containing solutions. After reaction at 60 °C for 2 h, CuO nanoflowers with assembled grass-like sheets were obtained. The longitude and transverse dimensions of the sheets were about 300 and 700 nm, respectively.

As mentioned above, thanks to the mild reaction conditions, mostly solution-based synthesis methods are used to prepare CuO materials with certain structures in a large scale. However, it always takes some time to separate the target product from the solution, which lowers the economy to some extent.

2.2.2 Solid-state methods

Compared with solution-based methods, separation of the final product and the supernatant can be avoided with solid-state methods, which saves time in obtaining the target materials. Solid state reaction and thermal oxidation of copper substrates are the main strategies used to successfully synthesize CuO nanostructures. Xu et al. (1999) used a one-step solid state reaction to prepare CuO particles. In this case, $CuCl_2$

was adopted as the copper precursor and NaOH for precipitation. After grinding for 30 h, CuO was formed, as evidenced by the color change of the products from green to black. Similarly, Abboudi et al. (2011) prepared copper oxalate through the reaction between $Cu(NO_3)_2$ and oxalic acid, and obtained CuO materials with calcination at high temperatures. In contrast, Balamurugan et al. (2001) used a conventional activated reactive evaporation (ARE) setup to prepare CuO particles. Briefly, copper vapor is passed through oxygen plasma with an oxidation reaction taking place; the produced CuO particles are then deposited in the chamber. Jiang et al. (2002) heated the cleared Cu substrates at between 400 and 700 °C in air for 4 h and found that CuO nanowires grew perpendicular to the substrate surface. The diameter centered in the range of 30–100 nm and the length up to <15 μm. The vapor-solid (VS) mechanism, rather than the vapor-liquid-solid (VLS) mechanism, was dominant in the growth process of CuO nanowires.

2.2.3 Electrochemical methods

Apart from solution-based and solid-state methods, electrochemical techniques are also accepted to be an excellent way to prepare CuO nanomaterials, due to their merits of simplicity and a mild synthesis condition. Using these techniques it is also easy to control the morphology and size of the obtained products through tuning the experimental parameters, such as the current density and voltage. Yuan et al. (2007) developed an electrochemical route to prepare CuO materials with various morphologies. Here, $NaNO_3$ solution was taken as the electrolyte and metallic copper as the sacrificial anode. When at a low current density, uniform and mono-dispersed CuO rods or spindles were produced. When the current density was excessively high, irregular-shaped crystals were formed (Fig. 4). This is because the growth of CuO followed three steps. First, $Cu(OH)_2$ was generated, then $Cu(OH)_2$ was dehydrated to tiny CuO particles. Finally, the formed CuO particles aggregated to form nanorods or nanospindles. As the current density was low, the rate of formation of CuO was at relatively low level, which resulted in a low concentration of CuO particles in the electrolyte, and consequently favored oriented aggregation with regular-shaped CuO materials produced. In contrast, a high current density would create a large amount of CuO particles and thus a random aggregation to form irregular-shaped crystals. Toboonsung and Singjai (2011) also used an electrochemical technique to synthesize CuO nanostructures. Stainless steel was adopted as the cathode, and copper plates as the anode. Deionized water was used as the electrolyte. Through tuning the voltage, electrode separation and deposition time, the production scale and physical structures of CuO nanorods and bundles could be well controlled. Similarly, Ulyankina et al. (2018) synthesized CuO powders via an electrochemical method, and by changing the average current density and the duty cycle, Cu_2O octahedra, Cu_2O polyhedral decorated with CuO, and Cu_2O-CuO composites were successfully prepared.

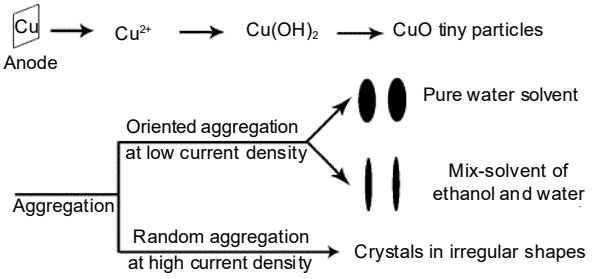

Fig. 4 Scheme of the controllable synthesis of CuO nanostructures. Reprinted from (Yuan et al., 2007), Copyright 2007, with permission from Elsevier

3 Hg^0 removal performance of CuO-based adsorbents

3.1 Supported CuO-based adsorbents

Here, CuO was used mainly as the active component and loaded on certain supports. To be the support of an adsorbent, a material should have the following characteristics. First, a relatively large specific surface area is essential so that the active species can be well-dispersed. Second, the material should have satisfactory stability, to help stabilize the supported active components. Finally, anti-poisoning ability is needed to ensure the long-run of an adsorbent. Among the various materials, carbon, zeolites, and metal oxides are recognized as typical adsorbent supports. Table 2 summarizes the Hg^0 removal performance of some typical adsorbents.

3.1.1 CuO/Carbon-based adsorbents

As a commonly used porous material, activated carbon (AC) shows good potential for the abatement

Table 2 Hg^0 removal performance of some typical adsorbents

Adsorbent	Flue gas composition	$C_{in\,Hg^0}$ (μg/m^3)	Flow rate (mL/min)	Temperature (℃)	Q (mg/g)	η (%)	Reference
CuO/AC	N_2+50 ppm HCl	21	105	180	–	49	Wang et al. (2012)
CuO-MnO_2/AC-H	N_2+5% O_2+500 ppm NO	50	300	200	–	92	Zhao et al. (2019)
Cu-Zr_x/Cl-BC	N_2+6% O_2	90	200	120	–	98.87	Tang et al. (2018)
CuFe/WSWU	N_2+5% O_2+400 ppm NO+600 ppm SO_2+4% H_2O	65	800	130	2.276	90.58	Yang W et al. (2019)
CuO/g-C_3N_4	N_2	50	1200	160	–	98.9	Liu et al. (2018a)
CuCe/ZSM-5	N_2	–	1200	210	–	98.4	Liu DJ et al. (2017)
Cu/HZSM-5	N_2+5% O_2+1000 ppm NO+1200 ppm NH_3+12% CO_2	20.02	500	250	–	90.2	Fan et al. (2012)
CuO/TiO_2	N_2+4%O_2+5 ppm HCl	150	700	50–300	–	>98	Xu et al. (2014)
CuO-CeO_2/TiO_2	N_2+4%O_2+1000 ppm NO+1000 ppm NH_3	75	1000	200	–	99	Li et al. (2017)
$CuMnO_x$/Al_2O_3	N_2	11600	83.3	ambient	–	About 100	Zhao et al. (2017)
CuO-MnO_2-Fe_2O_3/γ-Al_2O_3	N_2+5% O_2+10 ppm HCl+200 ppm NO+400 ppm SO_2+8% H_2O	75	1000	300	–	>70	Wang et al. (2013)
Cu-MOF	N_2	50	1000	120	123.5	>90	Zhang et al. (2021b)
Fe-Cu-MOF	N_2	50	1000	120	12.27	About 80	Zhang et al. (2021a)
Mn_xCu_y-MATP	N_2+6% O_2	55	1000	150	–	91.1	Long et al. (2022)
$CuMn_xO_y$	N_2+4% O_2	70	1000	50–250	–	>80	Yang R et al. (2019)
$CuMn_2O_4$	N_2+20% H_2+20% CO+400 ppm H_2S+10 ppm HCl	50	1000	200	–	>95	Wang Z et al. (2020)

$C_{in\,Hg^0}$ represents the inlet concentration of Hg^0 (μg/m^3); Q represents the Hg^0 capture capacity (mg/g); η represents the Hg^0 removal efficiency (%). ppm: 10^{-6}; MOF: metal organic frameworks; WSWU: wheat straw char activated by water stream and microwave and ultrasonicated; MATP: magnetic attapulgite

of Hg^0 owing to its advantages of satisfactory mechanical strength and wide availability. Wang et al. (2012) prepared CuO/AC adsorbents using the wet impregnation method and tested their performance. They found that the capability of CuO/AC for Hg^0 abatement was elevated by increasing the loading of CuO (1%–20% (in weight)), and at 180 ℃ the Hg^0 removal capability reached a peak value of *ca.* 38% (120–200 ℃). However, there are still some problems that need to be addressed: (1) Would the Hg^0 removal capability continue to increase with further increases in the loading of CuO? (2) Would the performance of CuO/AC exceed that of virgin CuO and AC? Based on CuO/AC-based adsorbents, Zhao et al. (2019) modified CuO/AC-H adsorbents with MnO_2 and achieved more than 90% Hg^0 removal efficiency at 200 ℃ as 5% MnO_2 was added. Here, AC-H was related to HNO_3-treated activated carbon. It was claimed that both lattice oxygen and reactive Mn-related intermediates had a positive effect on Hg^0 abatement. Apart from AC, bio-char (BC) has also received considerable attention for Hg^0 removal because of its environmental protection and low cost. Tang et al. (2018) used Cl^- activated bio-char as the support and CuO-ZrO_2 mixed oxides as the active species. When the loading amount of CuO-ZrO_2 increased to 10%, nearly 100% Hg^0 removal efficiency was reached and was maintained over 80% as the temperature was elevated to 240 ℃. It was proposed that interactions between CuO and ZrO_2, resulting in stronger oxidizability and improved texture properties, contributed to the superior performance of the Cu-Zr_{10}/Cl-BC adsorbent. Considering the separation problem of the spent adsorbents from fly ashes, Yang W et al. (2019) developed magnetic Fe-Cu oxide doped bio-char adsorbents by microwave/ultrasound activation. When the molar ratio of Cu/Fe was fixed at 0.3 and the loading value of Fe-Cu oxide raised to 10%, the average Hg^0 removal efficiency reached 90.58% at 130 ℃. The microwave and steam activation optimized the pore structures of the adsorbents, thereby promoting Hg^0 removal. This adsorbent also has a certain magnetic property, suggesting that it could be

effectively separated from the flue gas using simple physical methods.

Graphitic carbon nitride (g-C_3N_4), a typical kind of 2D carbon material, is beginning to be used as a support for Hg^0 removal owing to its high chemical and thermal stability, and abundant feedstock. When CuO was introduced as the active species, nearly 100% Hg^0 removal efficiency was obtained at between 80 and 200 ℃, which was almost double that of raw g-C_3N_4 (Liu et al., 2018a). During the Hg^0 removal process, Hg^0 was activated mainly by the chemisorbed oxygen, which originated from the O-C-N of g-C_3N_4 and the lattice oxygen of CuO. Adding CuO can efficiently activate g-C_3N_4 through the Mott-Schottky effect at the interface of CuO and g-C_3N_4, thereby significantly improving the Hg^0 removal capability (Liu et al., 2018b).

3.1.2 CuO/Zeolite-based adsorbents

Owing to their large specific surface area, abundant pore structures, and plentiful acid sites, zeolites are now accepted as another appropriate adsorbent support for Hg^0 removal. As in other pollutant removal reactions, ZSM-5 is used as the support with some metal oxides introduced as the active species and promoters. In the case of CuO/ZSM-5 adsorbent, about 70% Hg^0 removal efficiency was reached at 120 ℃. When CeO_2 or La_2O_3, the traditional promoters, were added, adsorbent Hg^0 capture performance was elevated to different extents (Liu DJ et al., 2017). The ability to remove Hg^0 composites increased by about 60% after introducing 50% CeO_2, and by 18% after adding 10% La_2O_3. This could be attributed to a cooperative effect between CuO and the doped promoter.

Apart from the properties of the promoters, the loading of CuO and the molar ratio of Si/Al also significantly affected the activity of the adsorbents (Fan et al., 2012). When the Cu loading value was elevated, adsorbent Hg^0 removal efficiency showed an upward trend, reaching a peak value of about 90% as the loading value of Cu reached 6% (in weight). Further increases in the loading value of Cu led to a decline in Hg^0 removal efficiency. This could be ascribed to the destruction of the tiny pores of the walls and blockage of internal porosity of the material by the excess doped copper. Unlike other researchers, Galloway et al. (2018) discovered that introducing copper species increased the Hg^0 removal efficiency of SSZ-13 only from 58.9% to 61.7%, demonstrating that SSZ-13 itself was primarily responsible for the abatement of Hg^0, and that CuO acted only as a promoter-like substance. As the molar ratio of Si/Al increased from 25 to 100, the adsorbent Hg^0 removal capability continuously decreased. This could be explained by a decline in the concentration of Cu^+, which was responsible for the high Hg^0 removal by the materials, as the Si content increased.

3.1.3 CuO/Metal oxide-based adsorbents

TiO_2 and Al_2O_3 are the main metal oxide supports used for Hg^0 removal because of their acceptable thermal stability and relatively large specific surface area. Xu et al. (2014) synthesized CuO/TiO_2 using a wet impregnation method. By changing the loading of CuO, 7% CuO/TiO_2 was found to be the optimal material, with an Hg^0 removal efficiency of 98% at between 50 and 300 ℃. Li et al. (2017) observed that the Hg^0 removal efficiency of CuO/TiO_2 increased from 90% to 99% at 200 ℃ with the modification of CeO_2. The elevated Hg^0 removal efficiency of CeO_2-CuO/TiO_2 could be explained mainly by the synergistic effect of copper oxide and cerium oxide promoting the formation of active chemisorbed oxygen, thereby accelerating the oxidation of Hg^0. Like TiO_2, adsorbents with Al_2O_3 as the support also showed good prospects for application. Zhao et al. (2017) impregnated CuO and MnO_2 onto an Al_2O_3 support surface to form CuO-MnO_2/Al_2O_3 adsorbent. The supported bimetallic adsorbent performed better than the monometal oxide adsorbents CuO/Al_2O_3 and MnO_2/Al_2O_3. This is because although MnO_2 was a strong oxidant, its oxidation rate was quite low, and the added CuO accelerated the oxidation process, thereby achieving an elevated Hg^0 pick capacity. As the content of CuO and MnO_2 reached 20%, the adsorbent showed an Hg^0 pick capacity of 12% (in weight), and the Hg^0 concentration could be reduced from more than 11600 to 10^{-10} in a single pass. By modifying CuO-MnO_2/Al_2O_3 with Fe_2O_3, over 70% removal efficiency was obtained in the first 10 h and no deactivation took place in a 3-d run, which suggests good potential for industrial applications (Wang et al., 2013).

3.1.4 Other CuO-supported adsorbents

Faced with the drawbacks of some traditional materials, such as their low-density of active sites and

low adsorption capacity, porous metal organic frameworks (MOF), are attracting increasing attention in catalysis, adsorption and separation due to their open active sites, abundant functional groups and large specific surface area. Zhang et al. (2021b) prepared Cu-MOF materials using an ultrasonic-assisted hydrothermal method and found that the resulting adsorbent had an average Hg^0 removal efficiency of >90% and a equilibrium adsorption capacity of 123.5 mg/g, which is much higher than that of some commercial activated carbon materials. Later, Zhang et al. (2021a) used iron species to modify Cu-MOFs and obtained bimetallic iron-copper based MOFs. Compared with Cu-BTC and Fe-MIL-53, the Hg^0 removal efficiency of FeCu-MOFs was almost doubled. The synergistic effect of iron and copper species facilitated the electron transfer process. This helped to provide an increased number of active sites and hence contributed to a satisfactory Hg^0 removal performance. Apart from MOFs, attapulgite (ATP) could be an appropriate material for Hg^0 removal due to the advantages of satisfactory thermal stability and large specific surface area. When modified with FeO_x, MnO_x, and CuO, adsorbent Hg^0 conversion showed an upward trend (Long et al., 2022). Here, FeO_x was regarded as the magnetic source, while MnO_x and CuO functioned as the active components for the oxidation of Hg^0. As the CuO loading reached 5%, over 90% Hg^0 removal efficiency was obtained. Further increases in the CuO content led to a decline in Hg^0 conversion, as excess CuO would cover the active sites of the adsorbents, thus impairing the Hg^0 removal process.

3.2 CuO mixed oxide-based adsorbents

Unlike the supported CuO adsorbents, CuO mixed oxides are always synthesized using co-precipitation or sol-gel methods. The homogeneous dispersion of the components ensures the sufficient occurrence of chemical interactions. The different valence states and radii of the constituent metal atoms promote the formation of surface oxygen vacancies to activate gaseous O_2 and the distortion of the lattice to bring about an improved texture structure. This somehow facilitates the capture of Hg^0. MnO_2, a typical metal oxide, is recognized as an appropriate dopant for the optimization of the adsorbent physicochemical properties because of its abundant surface vacancies and variable types of labile oxygen. Given that CuO is partially substituted by MnO_2, an increase in the adsorbent Hg^0 removal efficiency occurs. The adsorbent showed the best Hg^0 capture performance when 40% (in weight) CuO was replaced. About 70% Hg^0 removal efficiency could be maintained after 3 h. Further increasing the substitution of CuO led to a reduction in Hg^0 uptake. This could be ascribed to the formation of $CuMnO_2$ phase in the Mn-modified sample. The high valence of Mn facilitates the oxidation of Hg^0, and CuO accelerates the transformation of Mn from a low to a high valence state (Fig. 5). This was primarily responsible for the elevated Hg^0 removal performance of 40% MnO_2-modified adsorbent (He et al., 2018). In view of the superior Hg^0 removal performance of Mn-Cu mixed oxides, Yang R et al. (2019) synthesized a series of $Cu_xMn_{3-x}O_4$ materials using the sol-gel method. Hg^0 capture capability increased with increasing Cu content; over 95% Hg^0 removal efficiency was obtained between 50 and 350 °C when the x value was equal to 1. The higher concentrations of surface copper species and chemisorbed oxygen, together with the larger specific surface area, contributed to the efficient abatement of Hg^0 from the flue gas. Later, Wang Z et al. (2020) compared the Hg^0 capture performance of $CuMn_2O_4$ with that of $NiMn_2O_4$ and $ZnMn_2O_4$. They found that $CuMn_2O_4$ spinel still had a higher Hg^0 adsorption capability: over 95% Hg^0 removal efficiency was observed at 200 °C, about 30% higher than that of $NiMn_2O_4$ and $ZnMn_2O_4$.

4 Effects of gas components

In general, apart from N_2 and O_2 which account for about 80% of real coal-fired flue gas, there are certain amounts of NH_3, SO_2, NO, HCl, and H_2O. O_2 is the gas component typically involved in the evaluation of adsorbent Hg^0 removal performance under ideal conditions, and is proven to promote the capture of Hg^0. This is because O_2 can replenish the consumed lattice or chemisorbed oxygen species and re-oxidize the reduced metal ions. This accelerates the oxidation of Hg^0 and consequently facilitates the removal of Hg^0 (Zhang et al., 2021a). Like O_2, some other species, including SO_2 and NO, would also have some impact on the Hg^0 capture capability of adsorbents. This has been extensively studied by many researchers. Therefore, in this section, the effects of these other gas species on Hg^0 removal by some typical materials is summarized (Table 3).

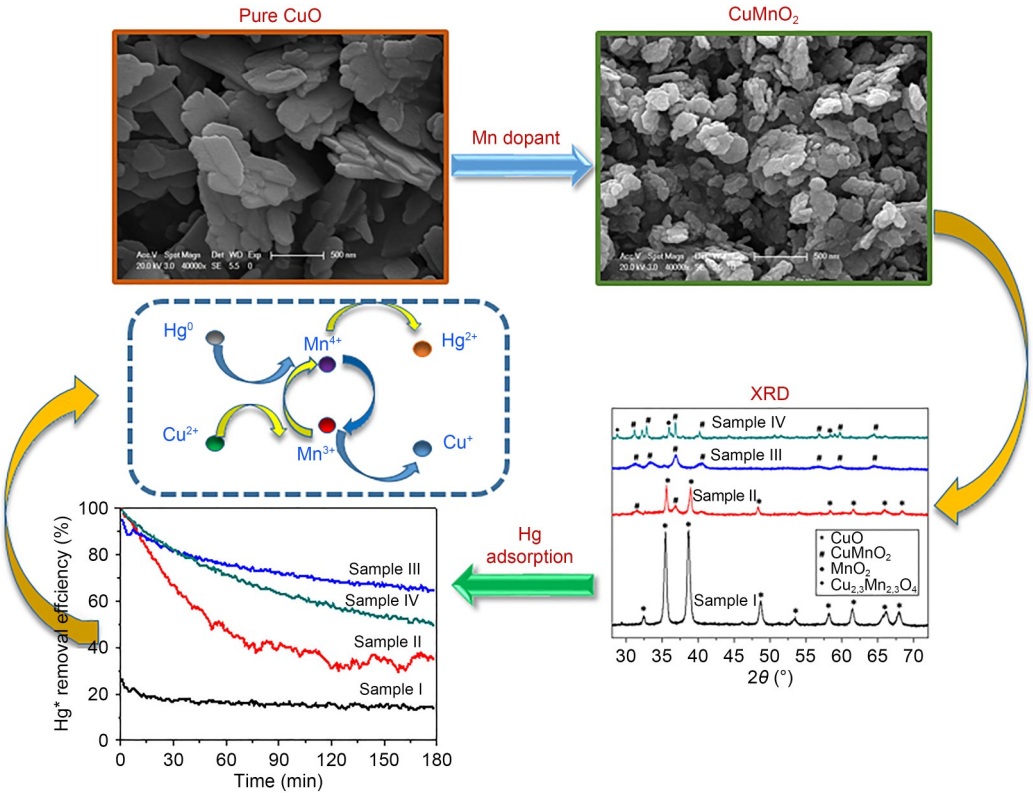

Fig. 5 Physicochemical properties of CuO and MnO_2-modified CuO materials. Reprinted from (He et al., 2018), Copyright 2018, with permission from Elsevier

Table 3 Effects of certain gas species on Hg^0 removal performance by some typical materials

Adsorbent	Flue gas composition	$C_{in\ Hg^0}$ (μg/m³)	Flow rate (mL/min)	Temperature (℃)	η (%)	Reference
Cu-MOFs	N_2	50	1000	120	91.8	Zhang et al. (2021b)
	N_2+4% O_2	50	1000	120	95.2	
	N_2+50 ppm NO	50	1000	120	98.5	
	N_2+600 ppm NO	50	1000	120	96.4	
	N_2+10 ppm HCl	50	1000	120	98.6	
	N_2+20 ppm HCl	50	1000	120	99.2	
	N_2+50 ppm SO_2	50	1000	120	91.5	
	N_2+800 ppm SO_2	50	1000	120	89.6	
	N_2+5% H_2O	50	1000	120	95.9	
CuFe/WSWU	N_2+400 ppm NO+600 ppm SO_2+4% H_2O	65	800	130	81.34	Yang W et al. (2019)
	N_2+400 ppm NO+600 ppm SO_2+4% H_2O+2% O_2	65	800	130	87.08	
	N_2+400 ppm NO+600 ppm SO_2+4% H_2O+10% O_2	65	800	130	93.31	
	N_2+600 ppm SO_2+4% H_2O+5% O_2	65	800	130	85.28	
	N_2+200 ppm NO+600 ppm SO_2+4% H_2O+5% O_2	65	800	130	88.77	
	N_2+800 ppm NO+600 ppm SO_2+4% H_2O+5% O_2	65	800	130	93.96	
	N_2+400 ppm NO+4% H_2O+5% O_2	65	800	130	95.98	
	N_2+400 ppm NO+1800 ppm SO_2+4% H_2O+5% O_2	65	800	130	81.85	
	N_2+400 ppm NO+600 ppm SO_2+5% O_2	65	800	130	90.58	
	N_2+400 ppm NO+600 ppm SO_2+12% H_2O+5% O_2	65	800	130	71.58	

(To be continued)

Table 3 (continued)

Adsorbent	Flue gas composition	$C_{in\ Hg^0}$ (μg/m^3)	Flow rate (mL/min)	Temperature (℃)	η (%)	Reference
CuCe/RSU	N_2+600 ppm SO_2+400 ppm NO+1.5% H_2O	50	800	150	46.91	Xu et al. (2018)
	N_2+15% O_2+600 ppm SO_2+400 ppm NO+1.5% H_2O	50	800	150	95.26	
	N_2+5% O_2+600 ppm SO_2+1.5% H_2O	50	800	150	44.79	
	N_2+5% O_2+600 ppm SO_2+800 ppm NO+1.5% H_2O	50	800	150	94.74	
	N_2+5% O_2+400 ppm NO+1.5% H_2O	50	800	150	87.73	
	N_2+5% O_2+400 ppm NO+1200 ppm SO_2+1.5% H_2O	50	800	150	37.11	
	N_2+5% O_2+600 ppm SO_2+400 ppm NO	50	800	150	93.37	
	N_2+5% O_2+600 ppm SO_2+400 ppm NO+8% H_2O	50	800	150	60.74	
Cu/ZSM-5	N_2+10% O_2	20	1000	200	85	Zhang HC et al. (2020)
	N_2+10% O_2+100 ppm SO_2	20	1000	200	75	
	N_2+10% O_2+100 ppm SO_x (12 ppm SO_3)	20	1000	200	89	
	N_2+10% O_2+100 ppm SO_x (21 ppm SO_3)	20	1000	200	95	
	N_2+10% O_2	20	1000	400	55	
	N_2+10% O_2+100 ppm SO_2	20	1000	400	52	
	N_2+10% O_2+100 ppm SO_x (21 ppm SO_3)	20	1000	400	90	
	N_2+10% O_2+1000 ppm SO_2	20	1000	200	49	
	N_2+10% O_2+1000 ppm SO_x (49 ppm SO_3)	20	1000	200	65	
	N_2+10% O_2+1000 ppm SO_x (96 ppm SO_3)	20	1000	200	84	
MnCu-MATP	N_2	55	1000	150	81.1	Long et al. (2022)
	N_2+6% O_2	55	1000	150	91.1	
	N_2+500 ppm NO	55	1000	150	94.5	
	N_2+500 ppm NO+6% O_2	55	1000	150	98.4	
	N_2+10 ppm HCl	55	1000	150	90.9	
	N_2+10 ppm HCl+6% O_2	55	1000	150	96.5	
	N_2+20 ppm HCl+6% O_2	55	1000	150	98.2	
	N_2+1000 ppm SO_2+6% O_2	55	1000	150	87.1	
	N_2+1500 ppm SO_2+6% O_2	55	1000	150	84.3	
	N_2+2% H_2O+6% O_2	55	1000	150	88.2	
	N_2+5% H_2O+6% O_2	55	1000	150	86.3	
	N_2+8% H_2O+6% O_2	55	1000	150	83.1	
MnCe/WSU	N_2+5% O_2+600 ppm SO_2+400 ppm NO+1% H_2O	55	800	150	83.6	Yang W et al. (2017)
	N_2+600 ppm SO_2+400 ppm NO+1% H_2O	55	800	150	37.6	
	N_2+9% O_2+600 ppm SO_2+400 ppm NO+1% H_2O	55	800	150	87.0	
	N_2+5% O_2+400 ppm NO+1% H_2O	55	800	150	86.7	
	N_2+5% O_2+300 ppm SO_2+400 ppm NO+1% H_2O	55	800	150	90.9	
	N_2+5% O_2+1200 ppm SO_2+400 ppm NO+1% H_2O	55	800	150	70.7	
	N_2+5% O_2+600 ppm SO_2+1% H_2O	55	800	150	49.2	
	N_2+5% O_2+600 ppm SO_2+800 ppm NO+1% H_2O	55	800	150	94.1	
	N_2+5% O_2+600 ppm SO_2+400 ppm NO	55	800	150	73.4	
	N_2+5% O_2+600 ppm SO_2+400 ppm NO+6% H_2O	55	800	150	47.5	
CuO/TiO_2	N_2+5% O_2+10 ppm HCl	106	500	100–400	About 100	Li et al. (2021)
	N_2+5% O_2+10 ppm HCl+50 ppm NH_3	106	500	100–400	About 100	
CuO-CeO_2/TiO_2	N_2	75	1000	200	80.0	Li et al. (2015)
	N_2+4% O_2	75	1000	200	89.0	
	N_2+1000 ppm NO	75	1000	200	84.6	
	N_2+1000 ppm NO+4% O_2	75	1000	200	98.2	
	N_2+1000 ppm NH_3	75	1000	200	45.5	
	N_2+1000 ppm NH_3+4% O_2	75	1000	200	89.7	
	N_2+1000 ppm NH_3+1000 ppm NO	75	1000	200	25.3	
	N_2+1000 ppm NH_3+1000 ppm NO+4% O_2	75	1000	200	58.0	

RSU: ultrasonicated rice straw chars; WSU: ultralsonicated wheat straw char

4.1 SO_2

SO_2, a typical acid gas, comes from the combustion of sulfur-containing coals and accounts for several hundreds of ppm in coal-fired flue gas. Because of its relatively high reactivity, most adsorbents are quite sensitive to SO_2. As reported in the literature, both adverse and positive impacts of SO_2 on the Hg^0 removal performance of the adsorbents have been detected.

Many papers have reported that SO_2 exerts a certain inhibitory effect on Hg^0 removal. Yang W et al. (2019) observed that given an increase in the SO_2 concentration, adsorbent Hg^0 removal efficiency showed a downward trend (Fig. 6). Xu et al. (2018) also discovered a negative impact of SO_2 on Hg^0 removal. Moreover, this adverse effect was enhanced as SO_2 was at a high concentration. It is well-accepted that formation of inert metal sulfates (Eqs. (1) and (2)) and competitive adsorption of Hg^0 and SO_2 on adsorbent active sites constitute the main reasons for the decline in Hg^0 removal efficiency in flue gas containing SO_2 (Wang HN et al., 2020; Ye et al., 2021).

$$CuO + SO_2 + O_2 \rightarrow CuSO_4, \quad (1)$$

$$MO_x + SO_2 + O_2 \rightarrow MSO_4. \quad (2)$$

Faced with this serious problem, some researchers optimized the formula of the adsorbents to improve SO_2 resistance. Mei et al. (2008) found that for $Cu_xCo_{3-x}O_4$ mixed oxide, the SO_2 anti-poisoning ability was improved, with the x value continuously increasing from 0.75 to 2.25. Yang R et al. (2019) used the "redox-precipitation" method to prepare MnO_2-CuO mixed oxide adsorbent, which showed some sulfur tolerance. After exposure to flue gas containing 1200 ppm SO_2 for about 50 min, adsorbent Hg^0 removal efficiency decreased by 15%. It was reported that CuO was preferentially consumed by SO_2 while MnO_2 survived and compensated for the loss of the active sites. Similarly, multiple active sites (Cu and C sites) and multiple oxidizing media (Cl and O) gave Cu-MOFs good tolerance to SO_2. Increasing the SO_2 content to 800 ppm reduced Hg^0 removal efficiency only slightly from 91.5% to 89.6% (Zhang et al., 2021b). Apart from the adsorbent formula, certain gas species can weaken the negative effect of SO_2 on Hg^0 removal. Chen et al. (2018) found that when HCl and O_2 in the flue gas were at a high concentrations, the influence of SO_2 could be negligible. Zhang HC et al. (2020) discovered that the addition of 21 ppm SO_3 was capable of increasing the Hg^0 removal efficiency of Cu/ZSM-5 from 82% to 95% at 200 °C. When the temperature was elevated to 400 °C, the positive effect of SO_3 on Hg^0 removal was enhanced. In this case, SO_3 could inhibit the adsorption of SO_2 and function as a new site to capture Hg^0 with the formation of $HgSO_4$.

Apart from the above-mentioned inhibitory impact, sometimes SO_2 can facilitate the removal of Hg^0 to some extent. Wang et al. (2013) observed that in the presence of 5% O_2, adding 1200 ppm SO_2 significantly lowered the outlet concentration of Hg^0 from about 63.0 to 47.1 μg/m^3. This is because CuO in CuO-MnO_2-Fe_2O_3/Al_2O_3 catalyzes the oxidation SO_2 to SO_3, which probably serves as an S-bonded chemisorption site for the abatement of Hg^0.

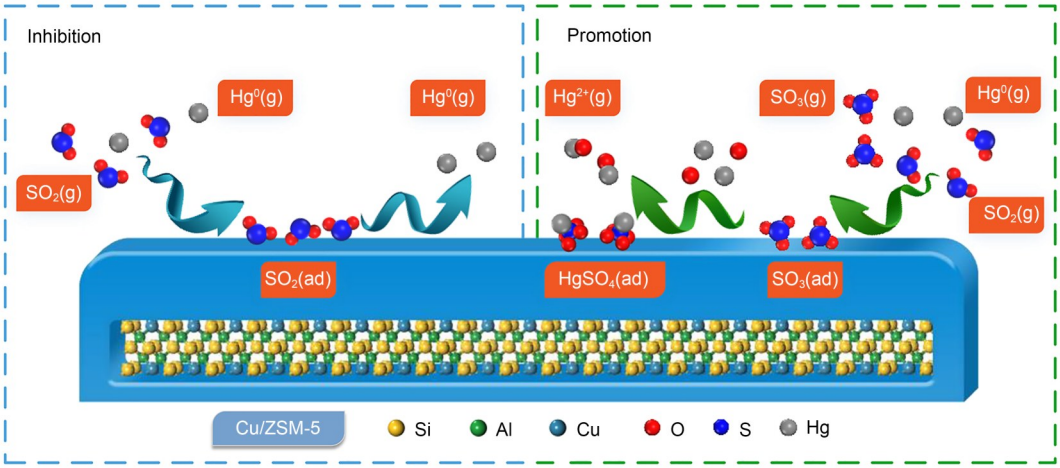

Fig. 6 Effect of SO_2 on Hg^0 removal over Cu/ZSM-5. Reprinted from (Zhang HC et al., 2020), Copyright 2020, with permission from Elsevier

4.2 NO

NO constitutes an inherent component of coal-fired flue gas. In view of its relatively high concentration and reactivity, NO was proven to be capable of influencing the Hg^0 removal performance of adsorbents to different extents. Like SO_2, both positive and negative effects on Hg^0 removal were observed. Long et al. (2022) found that NO could significantly promote the capture of Hg^0 over MnCu-MATP adsorbent. Purging 500 ppm NO elevated the Hg^0 removal efficiency from 81.1% to 94.6%, which further increased to 98.4% with 6% O_2. It was claimed that the NO^+, NO_3^-, and NO_2, formed through reaction between NO and adsorbent oxygen species, were primarily responsible for the promoted oxidation of Hg^0 to HgO, thereby facilitating the removal of Hg^0 (Eqs. (3)–(6)). After increasing the NO concentration to 1000 ppm, no obvious variation in the adsorbent Hg^0 removal performance could be detected. Xu et al. (2018) also observed that as the NO concentration increased from 0 to 800 ppm, the Hg^0 removal efficiency of CeO_2- and CuO-modified rice straw chars increased from 44.79% to 94.74%. The formation of reactive nitrates or nitrites contributed to the improved Hg^0 removal performance of the adsorbents (Eqs. (3)–(6)). In contrast, Zhang et al. (2021b) discovered that when the concentration of NO increased from 50 to 600 ppm, the Hg^0 removal efficiency of Cu-MOF adsorbent declined slightly. The excessive NO would lead to competitive adsorption with Hg^0, which would limit any further facilitation of Hg^0 removal.

$$NO + \frac{1}{2}O_2 \rightarrow NO_2, \tag{3}$$

$$Hg^0 + NO_2 \rightarrow HgO + NO, \tag{4}$$

$$Hg^0 + 2NO_2 + O_2 \rightarrow Hg(NO_3)_2, \tag{5}$$

$$Hg^0 + 2NO + 2O_2 \rightarrow Hg(NO_3)_2. \tag{6}$$

4.3 H_2O

H_2O, accounting for around 10% of real coal-fired flue gas, is another primary gas component with a crucial role to play in air pollutant abatement reactions. It is well recognized that in most cases H_2O has an adverse impact on the adsorption of Hg^0. For most MOF-, zeolite-, and carbon-based adsorbents, water vapor poisoning phenomena can always be observed (Chen et al., 2018; Xu et al., 2018; Long et al., 2022). Similar to the negative effect of SO_2, competition for the active sites over the adsorbents between Hg^0 and H_2O mainly explains the decline in Hg^0 removal efficiency in the presence of H_2O. In contrast, Yang W et al. (2019) discovered that for iron-copper oxide modified porous char, introducing 4% H_2O had a certain promotional effect on Hg^0 removal. The hydroxyl radicals originating from the decomposition of water molecules would participate in the oxidation of Hg^0 to HgO, which mainly contributes to the increased Hg^0 removal efficiency (Eqs. (7) and (8)). After increasing the H_2O content to 12%, similar phenomena could be obtained, showing a downtrend in the removal efficiency of Hg^0. Formation of a water film on the adsorbent surface could also explain the inhibitory effect of H_2O on Hg^0 abatement.

$$H_2O \rightarrow H + OH, \tag{7}$$

$$OH + Hg^0 \rightarrow HgO + H. \tag{8}$$

4.4 HCl

HCl, considered a typical acid gas with high reactivity, accounts for about tens of ppm in real coal-fired flue gas, and also affects the Hg^0 removal performance of the adsorbents to some extent. Most researchers observed that purging a certain amount of HCl into the reaction system could elevate the Hg^0 removal efficiency (Xu et al., 2014, 2018; Du et al., 2015; Zhang et al., 2021a). It was claimed that HCl would interact with the adsorbent chemisorbed oxygen to form active chlorine species, which then accelerates the oxidation of Hg^0 and enhances its removal (Eqs. (9)–(14)) (Yang YJ et al., 2017). Some researchers found that HCl could have an inhibitory effect on Hg^0 removal under certain conditions. Wang Z et al. (2020) observed that the Hg^0 removal efficiency of $CuMn_2O_4$ spinel adsorbent obtained in the presence of 10 ppm HCl increased by 14.7% compared with that obtained in N_2. After further increasing the HCl concentration, a decline in the adsorbent Hg^0 capture capability occurred. When an appropriate amount of HCl was added, formation of reactive chlorine species mainly contributed to the facilitated oxidation of Hg^0. When the concentration of HCl was excessively high, it could not be efficiently converted to active chlorine species because of the limited chemisorbed oxygen available. Thus, the residual HCl would occupy the surface active sites and consequently constrain Hg^0

capture (Yang et al., 2014). Similar phenomena were obtained by Wang et al. (2013). In the presence of O_2, an enhancement in Hg^0 removal took place through adding HCl. In contrast, without O_2, HCl inhibited the abatement of Hg^0. Formation of reactive chlorine species and competitive adsorption of HCl and Hg^0 could well explain the effect of HCl on Hg^0 removal over $CuO\text{-}MnO_2\text{-}Fe_2O_3/Al_2O_3$.

$$2HCl + O(s) \rightarrow 2Cl(ad) + H_2O, \quad (9)$$

$$Hg^0(ad) + Cl(ad) \rightarrow HgCl(ad), \quad (10)$$

$$Hg^0 + Cl(ad) \rightarrow HgCl(ad), \quad (11)$$

$$HgCl(ad) + Cl(ad) \rightarrow HgCl_2(ad), \quad (12)$$

$$Hg^0(ad) + 2Cl(ad) \rightarrow HgCl_2(ad), \quad (13)$$

$$Hg^0 + 2Cl(ad) \rightarrow HgCl_2(ad). \quad (14)$$

4.5 NH_3

NH_3, a typical reducing component from the $deNO_x$ systems, is also proven to significantly affect the Hg^0 removal process over the adsorbents. Unlike SO_2, NO, HCl, and H_2O, no promotional effect of NH_3 on Hg^0 removal has been reported. NH_3 exerts only a small positive effect, or even a negative effect, on the abatement of Hg^0. Wang et al. (2013) discovered that given a purge of 200 ppm NH_3 into the reactor, Hg^0 removal efficiency declined by *ca*. 25%. Similarly, competition between Hg^0 and NH_3 for the active sites and surface oxygen can mainly explain the inhibitory impact of NH_3. Li et al. (2021) found that NH_3 had little effect on Hg^0 removal over CuO/TiO_2 (Fig. 7). It was claimed that CuO is a borderline acid, which weakly interacts with NH_3 leaving plenty of active sites available for Hg^0 removal. That enables CuO/TiO_2 to achieve excellent Hg^0 removal performance in the presence of NH_3 at lower temperatures. When the temperature increases, NH_3 would be oxidized to NO_2, which is the reactive species contributing to Hg^0 removal. Hence, a novel NH_3-tolerant ability is obtained. Over $CuO\text{-}CeO_2/TiO_2$, NH_3 also presented no obvious inhibitory effect on Hg^0 removal (Li et al., 2017). However, once NO and NH_3 were simultaneously added to the flue gas at a molar ratio of 1, deactivation of Hg^0 conversion occurred. In this case, NO and NH_3 could react directly with HgO to form Hg^0 and N_2. The reduced copper and ceria species in the selective catalytic reduction (SCR) reaction of NO would rob the oxygen species from HgO, resulting in a decline in Hg^0 removal efficiency. A similar adverse impact of SCR reactants (NO and NH_3) was also obtained over Cu-SSZ-13. Such knowledge is of fundamental importance for the simultaneous abatement of multi-air pollutants.

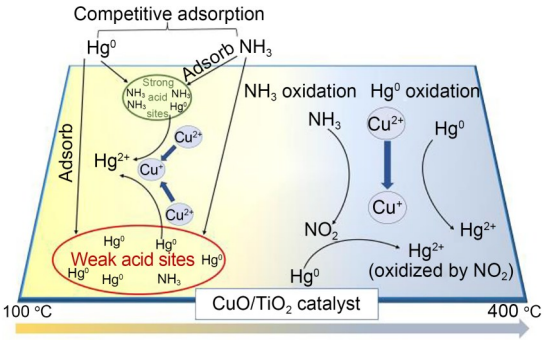

Fig. 7 Effect of NH_3 on Hg^0 removal over CuO/TiO_2. Reprinted from (Li et al., 2021), Copyright 2021, with permission from Elsevier

5 Hg^0 removal mechanisms

Both physisorption and chemisorption are involved in Hg^0 removal reactions (Yang W et al., 2017; Yang Y et al., 2019). At relatively low-temperatures, physisorption sometimes took place, during which process adsorbent surface vacancies were mainly involved (Yang et al., 2011a, 2011b). As the temperature rises, chemisorption becomes dominant. By tuning the components of the flue gas, different products can be obtained. Chen et al. (2018) found that in the absence of HCl, Hg^0 was removed mainly in the form of HgO. When HCl is present in the flue gas, Cu species in Cu-BTC adsorbent would interact with HCl to form an intermediate, namely CuCl or $CuCl_2$. Hg^0 could be oxidized with chemisorbed oxygen or activated chlorine species to form the final product, $HgCl_2$. Variation in the final product of the adsorbed mercury species indicated that purging HCl into the flue gas changed the intermediate in the Hg^0 capture process, which might have brought about the different removal mechanisms. Therefore, in this section, detailed Hg^0 removal routes over adsorbents in the presence or absence of HCl will be discussed.

5.1 Hg^0 removal mechanisms in the absence of HCl

When HCl is absent from the flue gas, the capture of Hg^0 is highly dependent on the reactivity of oxygen

species and the kinds of functional groups on the adsorbent surfaces. As a consequence, the main products of the captured mercury species are always HgO and Hg-OM (M represents the carbon functional groups). Xiang et al. (2012) used a density functional theory (DFT) method to investigate the adsorption mechanism of Hg^0 over CuO and observed that Hg^0 could physisorb onto the O-terminated surfaces, and chemisorb onto Cu-terminated CuO (110) surfaces (Fig. 8). Compared with physisorption, chemisorption plays a dominant role in Hg^0 capture. Chemisorption always involves certain mechanisms, such as Deacon and Mars-Maessen mechanisms, and thus provides some guidelines for the investigation of the Hg^0 capture route on adsorbents. Among all the sites, Cu_{sub} top was the most favorable for Hg^0 adsorption, with an adsorption energy of −116.76 kJ/mol. Yang et al. (2019c) studied the active sites and the Hg^0 adsorption mechanisms over $CuMn_2O_4$, a new kind of promising adsorbent. An excellent O_2-activation ability was found over $CuMn_2O_4$. The activation energy of the O_2 dissociation reaction over $CuMn_2O_4$ was calculated to be 6.31 kJ/mol. Both chemisorbed oxygen molecules (O_2^*) and atoms (O^*) coming from the dissociation of O_2 were involved in the oxidation of Hg^0. In the whole mercury adsorption-oxidation-desorption process, HgO desorption constituted the rate-determining step (Fig. 9). For $CuFe_2O_4$ adsorbent, the oxidation of the adsorbed Hg^0 (Hg^0(ad)) to the adsorbed HgO by chemisorbed oxygen was the rate-determining step in Hg^0 abatement cycles, owing to the higher energy barrier of 116.94 kJ/mol (Yang et al., 2022). These results revealed that variation in the formula of the adsorbents can change the energy barrier of certain elementary reactions, hence leading to the different rate-determining steps.

Apart from DFT methods, some characterization experiments were also proven to be effective to uncover the Hg^0 capture mechanisms over the adsorbents. Liu DJ et al. (2017) explored variation in the valence states of the serial elements in CuO/ZSM-5 and observed that the Mars-Maessen mechanism dominated in the Hg^0 capture cycles. The physisorption of Hg^0 on the adsorbent surface through the van de Waals force constituted the first step. Then lattice oxygen of the active component CuO was released and participated in the oxidation of Hg^0 to HgO, accompanied by the reduction of Cu^{2+} to Cu^+ (Eqs. (15)–(17)), which was regarded as the chemisorption process. Zhang et al. (2019) also observed that Cu^{2+} in CuO/montmorillonite acted as the active sites for the oxidation of Hg^0, and the adsorbed mercury species were present mainly in the form of HgO. Unlike virgin CuO or zeolite-based adsorbents, the complex physicochemical properties of carbon-based materials can make the adsorbed mercury species exist in various forms, thereby creating some different Hg^0 capture pathways. For copper-iron mixed oxide-modified biochar materials, some functional groups, namely carbonyl and carboxyl groups, could serve as the active sites to oxidize Hg^0 to Hg-OM compounds. Lattice oxygen and chemisorbed oxygen of CuO and Fe_2O_3 participates in the direct oxidation of Hg^0 to HgO (Eqs. (18)–(21)) (Jia et al., 2018), giving Fe-Cu/BC a satisfactory Hg^0 removal performance.

$$Hg^0(g) + \text{surface} \rightarrow Hg^0(s), \quad (15)$$

$$2CuO(s) \rightarrow Cu_2O + [O], \quad (16)$$

$$Hg^0(s) + [O] \rightarrow HgO(s), \quad (17)$$

$$Hg^0 + AC - \text{surface} \rightarrow Hg^0(ad), \quad (18)$$

$$Fe_2O_3 \rightarrow 2FeO + O, \quad (19)$$

$$2CuO \rightarrow Cu_2O + O, \quad (20)$$

$$Hg^0(ad) + O \rightarrow HgO(ad). \quad (21)$$

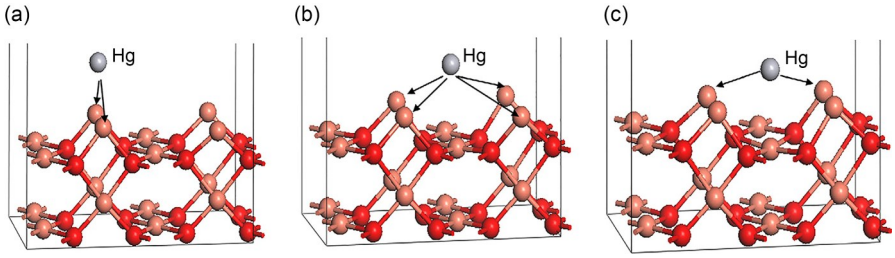

Fig. 8 Optimized geometries of Hg^0 adsorption on Cu-terminated CuO (110) surface: (a) Cu_{suf} top and bridge site; (b) Cu_{sub} top site; (c) hollow site. The salmon pink, red, and gray spheres denote Cu, O, and Hg atoms, respectively. References to color refer to the online version of this figure. Reprinted from (Xiang et al., 2012), Copyright 2012, with permission from Elsevier

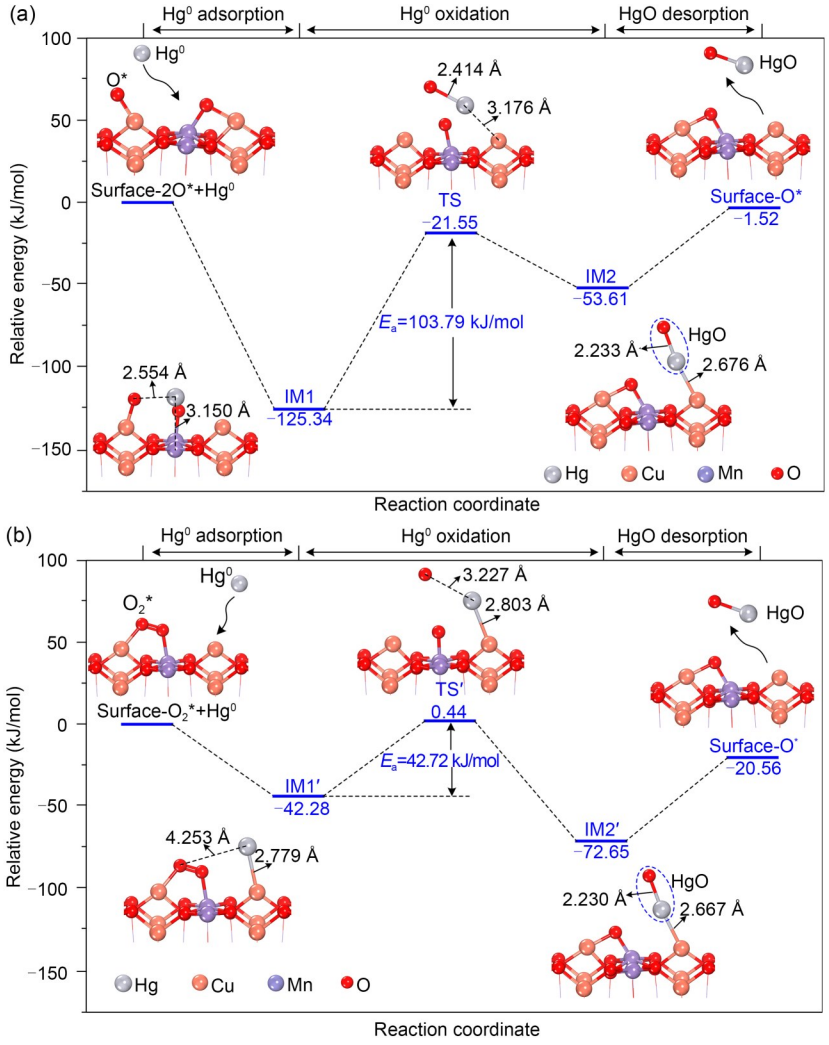

Fig. 9 Hg^0 removal mechanisms over $CuMn_2O_4$. The reaction pathways and relative energies for mercury oxidation by chemisorbed oxygen atom O^* (a) and oxygen molecule O_2^* (b) over $CuMn_2O_4$ surface. E_a: activation energy. Reprinted from (Yang et al., 2019c), Copyright 2019, with permission from American Chemical Society

5.2 Hg^0 removal mechanisms in the presence of HCl

When HCl is present in the flue gas, the as-formed chlorine species with a relatively high reactivity can interact with Hg^0, forming $HgCl_2$. Variation in the final products of the captured mercury species must originate from the changed intermediates and the potentially different reaction routes. Zhang et al. (2021b) concluded that the Hg^0 removal process over Cu-MOFs followed the Langmuir-Hinshelwood mechanism (Fig. 10). First, unsaturated active Cu or C sites were responsible for the physisorption of Hg^0, which was then oxidized to $HgCl_2$, with Cu^{2+} reduced to Cu^+. Finally, the reduced Cu^+ was re-oxidized by O_2 and HCl, forming a complete Hg^0 oxidation cycle. When iron species are introduced to form bimetallic adsorbents, the Langmuir-Hinshelwood mechanism was still found to dominate during the whole Hg^0 capture process (Eqs. (22)–(30)) (Zhang et al., 2021a). Zhang Q et al. (2020) used Hg balance, kinetics, and transient reactions to investigate the removal mechanisms of Hg^0 over CuO/TiO_2 in the presence of HCl. They discovered that HgO adsorbed on the adsorbent surface hardly reacted with HCl to form $HgCl_2$. Also, the reaction order of Hg^0 between 300 and 400 °C with respect to the concentration of gaseous Hg^0 was much lower than 1. This suggested that the Langmuir-Hinshelwood mechanism, rather than the Mars-Maessen, Deacon, or Eley-Rideal mechanisms, could explain the Hg^0 removal route on CuO/TiO_2, similar to the

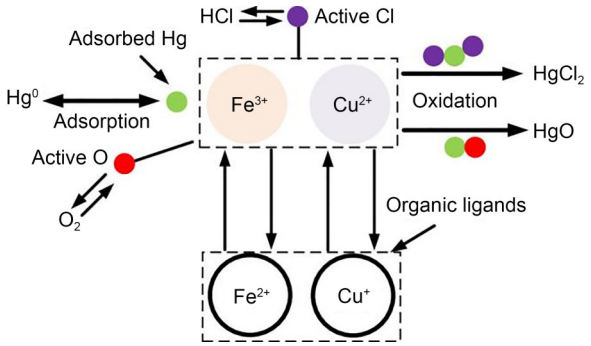

Fig. 10 Hg^0 removal mechanisms over CuFe-MOFs in the presence of HCl. Reprinted from (Zhang et al., 2021a), Copyright 2021, with permission from American Chemical Society

above-mentioned results. However, opposite conclusions were drawn by Du et al who suggested that the Mars-Maessen mechanism could explain the Hg^0 removal route over CuO_x-neutral Al_2O_3 (Du et al., 2015). Active chlorine species (Cl^-) were formed via the dehydrogenation of HCl, which then oxidized Hg^0 to $HgCl_2$. When the reaction temperature increased, the release step of Cl^- was accelerated, primarily contributing to an improved Hg^0 capture capability. In this process, CuO_x functioned as a catalyst through the redox shift of $Cu^{2+}\leftrightarrow Cu^+$.

$$Cu^{2+}+O^{2-}+HCl\leftrightarrow Cu^{+}+Cl^{-}+OH^{-}, \quad (22)$$

$$Cu^{+}+O^{2-}+HCl\leftrightarrow Cu^{0}+Cl^{-}+OH^{-}, \quad (23)$$

$$Cu^{+}+O_2\leftrightarrow Cu^{2+}+O^{2-}, \quad (24)$$

$$Cu^{0}+O_2\leftrightarrow Cu^{+}+O^{2-}, \quad (25)$$

$$OH^{-}+OH^{-}\leftrightarrow H_2O+O^{2-}, \quad (26)$$

$$Hg^{0}+Cl^{-}\leftrightarrow HgCl^{-}, \quad (27)$$

$$HgCl^{-}+Cl^{-}+e^{-}\leftrightarrow HgCl_2, \quad (28)$$

$$HgCl_2(g)\leftrightarrow HgCl_2(ad), \quad (29)$$

$$Hg+2HCl+\frac{1}{2}O_2\xleftrightarrow{CuO_x}HgCl_2+H_2O. \quad (30)$$

6 Simultaneous removal of multiple pollutants

Apart from Hg^0, other air pollutants, such as NO_x, VOCs, and carbon monoxide, are also present in real coal-fired flue gas. Considering the similar removal mechanisms of these pollutants, it has become popular to remove multiple pollutants simultaneously with the use of certain materials. The reduction of operating costs and space requirements further attracted attention to the simultaneous removal of multiple pollutants.

6.1 Simultaneous removal of Hg^0 and NO_x

Nitrogen oxides (NO_x) are another serious air pollutant emitted from power stations. Owing to the similar material properties, namely oxidizability and acidity, involved in the selective catalytic reduction of NH_3 and oxidation of Hg^0, it is reasonable to attempt to remove Hg^0 and NO_x simultaneously from coal-fired flue gas using an appropriate catalyst/adsorbent. Wang HY et al. (2019) modified the commercially used deNO_x catalyst, V_2O_5-WO_3/TiO_2, with CuO. When the content of CuO increased, catalyst Hg^0 removal efficiency first increased to the peak value of *ca.* 100% at temperatures of 280–360 °C, and then slightly decreased. A slight variation in the deNO_x efficiency was noted, with N_2 selectivity maintaining *ca.* 100%, indicating an excellent NO_x and Hg^0 abatement capability. Sun et al. (2021) prepared CuO/Fe-Ti and investigated its deNO_x and Hg^0 removal performance. In this case, Fe-Ti mixed oxide was taken as the support and CuO was recognized as the active species. When the CuO loading was increased, material SCR deNO_x activity always stayed at a satisfactory level. About 100% NO_x removal efficiency was obtained between 300 and 450 °C. The introduced CuO also facilitated the formation of Cl^* radicals, which overpowered the negative effect of the slightly inhibited physisorption of Hg^0, thus contributing to a high Hg^0 oxidation rate of 6.8–8.7 μg/(g·min). Similarly, Cu-Ce-Zr-O mixed oxide was deposited onto the Al_2O_3 support surface to obtain a catalyst to simultaneously remove Hg^0 and NO_x (Yue et al., 2019). With the molar ratio of Cu:Ce:Zr fixed to 1.40:0.55:0.25 and the loading amount of Cu-Ce-Zr-O mixed oxide set as 15%, deNO_x efficiency of 93% and Hg^0 removal efficiency of 85% were observed. Low crystallinity, optimized textural structures, strong acid properties, and oxidative ability mainly explained the excellent simultaneous Hg^0 and NO_x removal performance of the catalyst. Apart from the formula, the existing forms of the main active species, copper species, also significantly affected the performance of the materials. Wang Y et al. (2019) varied the content of Cu in Cu-SAPO-34 material and found that the Cu ions isolated inside the pores acted as the active sites for the SCR reactions, while crystallite CuO was primarily responsible for the oxidation of Hg^0. Through tuning the loading amount of Cu, both Cu^{2+} and CuO increased, leading to an increased removal efficiency of NO_x and Hg^0 (Fig. 11).

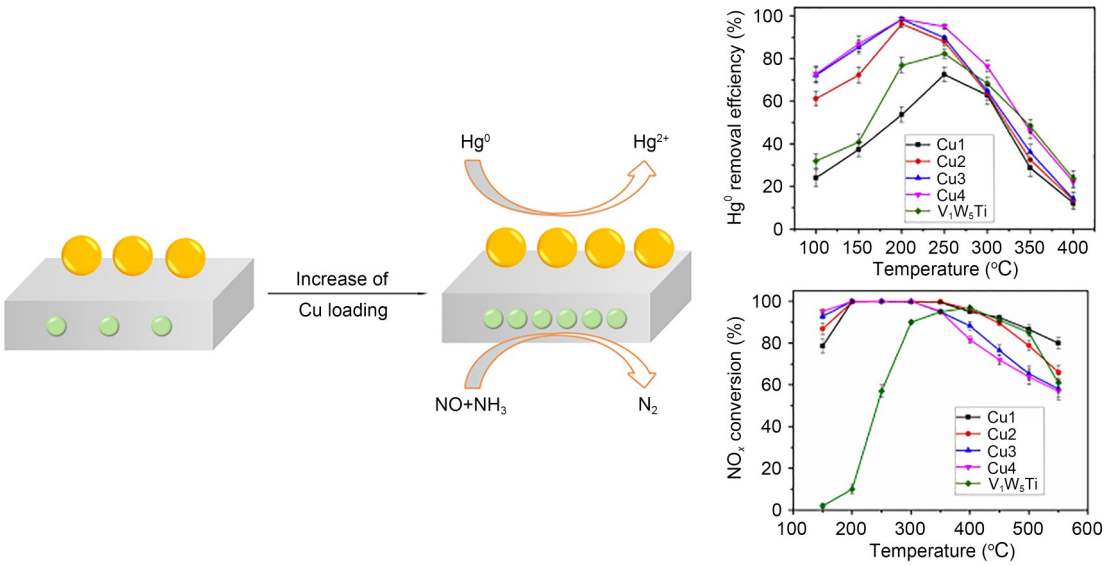

Fig. 11 NO_x conversion and Hg^0 removal efficiency over Cu-SAPO-34. Reprinted from (Wang Y et al., 2019), Copyright 2019, with permission from Elsevier

6.2 Simultaneous removal of Hg^0 and other air pollutants

Like Hg^0, CO is a toxic, persistent air pollutant that is of great harm to the environment. Considering that oxidative ability also plays a crucial role in the abatement of CO, it seems that the goal of simultaneous removal of Hg^0 and CO should be achievable. Gao et al. (2021) deposited the binary mixed oxide CuO_x-CoO_x onto an HNO_3-pretreated activated carbon surface to form CuO_x-CoO_x/AC_N catalyst. When the contents of CuO_x and CoO_x were set to 2% and 10%, respectively, complex oxides, including CuO, Cu_2O, Co_3O_4, Co_2O_3, and CoO phases, co-existed. In this catalyst, Co-species were responsible for the oxidation of CO, and Cu-species contributed to the removal of Hg^0. With increasing reaction temperature, CO removal efficiency exhibited an upward trend, which reached *ca.* 94.7% at 200 ℃. The effect of reaction temperature on the material Hg^0 removal performance was negligible.

Formaldehyde (HCHO), a typical kind of VOC, also constitutes a hazardous substance discharged from coal-fired power plants. Yi et al. (2018) adopted an impregnation method to synthesize Cu-Mn mixed oxides, supported on biochar materials, for the simultaneous removal of Hg^0 and HCHO. When the molar ratio of Cu/Mn was set to 1:1 and the mixed metal oxide loading value was fixed at 12%, the highest removal efficiencies of HCHO and Hg^0 (89% and 83%, respectively) were obtained at 175 ℃. The strong synergistic effect between MnO_2 and CuO_2 plays an important role in the abatement reaction of HCHO and Hg^0 because of the redox cycle of Mn^{4+}+Cu^+ ↔ Mn^{3+}+Cu^{2+}.

7 Hg^0 removal in WFGD

Through the use of adsorbents, Hg^0 in the flue gas can be oxidized to Hg^{2+}. When flue gas passes through electrostatic precipitators, some Hg^{2+} can be captured, leaving the residual Hg^{2+} to enter WFGD devices and finally be removed by the absorbents (Lim et al., 2020, 2021, 2022). When Hg^{2+} is dissolved, the existing reductive ligands and compounds reduce Hg^{2+} to Hg^0, resulting in the re-emission of Hg^0 (Eqs. (31)–(34)) (Hsu et al., 2021).

$$Hg^{2+}(aq)+SO_3^{2-}(aq)\rightarrow HgSO_3(aq), \quad (31)$$

$$HgSO_3(aq)+H_2O(aq)\rightarrow Hg^0(g)+SO_4^{2-}(aq)+2H^+(aq), \quad (32)$$

$$Hg^{2+}(aq)+2OH^-(aq)\rightarrow Hg(OH)_2(aq), \quad (33)$$

$$Hg(OH)_2(aq)+M^{n+}(aq)\rightarrow Hg^0(g)+MO(aq)+H_2O(aq). \quad (34)$$

Among the various processing parameters, pH, temperature, ion concentration, and metal concentration

have a significant impact on the amount of Hg^0 released (Hsu et al., 2021). When the pH value exceeds 6, SO_3^{2-} is favorable in solution and tends to react with Hg^{2+} to form the unstable product $HgSO_3$, which will spontaneously decompose to Hg^0 (Omine et al., 2012; Ma et al., 2014). With increasing SO_3^{2-} concentration, the formation of $Hg(SO_3)_2^{2-}$, which is less stable than $HgSO_3$, is facilitated, thus contributing to increased Hg^0 re-emission (Blythe et al., 2010). These two sulfite formation reactions are proven to be exothermic and spontaneous. Therefore, the decomposition of $Hg(SO_3)_2^{2-}$ and $HgSO_3$ will be promoted at a high temperature point (van Loon et al., 2001).

Chlorine compounds are a typical component of the absorbents and slurry of WFGD systems (11–15 g/L). Cl^- easily complexes with Hg^{2+} to form $HgCl^+$, $HgCl_2$, and $HgCl_3^-$, which have higher stability than $Hg(SO_3)_2^{2-}$ and $HgSO_3$. Cl^- can also compete with SO_3^{2-} to react with Hg^{2+} and thus interfere with the reaction between Hg^{2+} and SO_3^{2-} (Bessinger et al., 2012; Devarajan et al., 2018). Also, the formed $ClHgSO_3^-$ elevates the stability of Hg^{2+}, which can be regarded as an effective method to control the re-emission of Hg^0 in WFGD devices (Peng et al., 2016). Like Cl, Br, F, and I are also capable of exerting an inhibitory effect on Hg^0 re-emission. The effect of these halides follows the order I>Br>Cl>>F (Hsu et al., 2021).

As a typical component of flue gas, O_2 can indirectly affect the reduction of Hg^{2+} and the re-emission of Hg^0. The mostly accepted influence mechanism of O_2 is the oxidation of SO_3^{2-} in solution to SO_4^{2-}. Hg^{2+} first interacts with SO_3^{2-} forming $HgSO_3$, and then complexes with SO_4^{2-} to form a moderately stable product $HgS_2O_7^{2-}$, which consequently leads to a decline in the re-emission of Hg^0 (Chang et al., 2017; Hsu et al., 2019). Note that in the absence of SO_3^{2-}, an unstable product, $Hg(SO_4)_2$, will be produced through the complexation between two moles of SO_4^{2-} and one mole of Hg^{2+}, which in turn elevates the re-emission of Hg^0 (Powell et al., 2005). Like O_2, As compounds also exert dual effects on Hg^0 re-emission. When the concentration of As is in the range of 0.02–0.55 mg/L, $H_2AsO_3^-$ functions as a reducing agent to reduce Hg^{2+} to Hg^0. With the concentration of As shifting to 0.55–0.76 mg/L, a complexation reaction between two moles of $H_2AsO_3^-$ and one mole of Hg^{2+} occurs with the formation of stable $Hg(H_2AsO_3)_2$, making Hg^{2+} stay in the liquid phase (Liu et al., 2017). Unlike O_2 and As, Fe and Cu, the main metal components in coals, play only the role of a catalyst to reduce Hg^{2+} to Hg^0, which subsequently creates an increased Hg^0 re-emission (Bogacki et al., 2018; Gingerich et al., 2018).

Little information is available regarding economic analysis of the application of CuO-based materials for Hg^0 removal and effective absorption of Hg^0 in WFGD, and extensive research should thus be conducted (Choi et al., 2020; Lee et al., 2021, 2022).

8 Conclusions and perspectives

When the formula and preparation methods of adsorbents are properly selected, the corresponding physicochemical properties are greatly optimized, leading to an enhancement of Hg^0 capture capability. Considering that certain gas species somehow influence Hg^0 removal efficiency, appropriate modification should ensure the potential long-term operation of the adsorbents. Besides, by investigating Hg^0 abatement mechanisms under different conditions, the rate-determining step could be discovered, which can provide a guideline for the development of new adsorbents with excellent performance. In WFGD, once the reaction conditions, such as pH, temperature, ion concentration, and metal concentration, are optimized, the re-emission of Hg^0 can be inhibited, hence achieving a relatively high system Hg^0 removal efficiency.

At lab-scale, Hg^0 can be effectively captured, and even multiple air pollutants can be simultaneously removed by some reported materials. However, at pilot-scale and full-scale, there is still some doubt as to whether Hg^0 and other air pollutants can be thoroughly abated. The competitive adsorption mechanisms of multiple air pollutants onto the adsorbent surface active sites still needed to be explored. Knowledge of such effects would be beneficial for further increasing the corresponding pollutant removal efficiency. Apart from SO_2, NO, H_2O, NH_3, and HCl, there are other species in real coal-fired flue gas, such as arsenic, phosphorus, and lead compounds. The effects of these species on the adsorbent Hg^0 capture performance also needs investigation. Provided these species would deactivate the adsorbents, the related anti-poisoning and regeneration techniques should also developed to achieve the goal of the effective reduction of mercury emissions. Finally, a techno-economic assessment of

the application of CuO-based materials for Hg^0 removal and effective absorption of Hg^0 in WFGD should be carried out because knowledge of such effects lays a solid foundation for effective reduction of Hg^0 emissions.

Acknowledgments

This work is supported by the Scientific Research Foundation of China Jiliang University and the Zhejiang Provincial Natural Science Foundation of China (Nos. LQ22E060003 and LY22E040001).

Author contributions

Dong YE wrote the first draft of the manuscript. Xin LIU and Run-xian WANG helped to organize the manuscript. Dong YE, Xiao-xiang WANG, Hai-ning WANG, and Hui LIU revised and edited the final version.

Conflict of interest

Dong YE, Xiao-xiang WANG, Run-xian WANG, Xin LIU, Hui LIU, and Hai-ning WANG declare that they have no conflict of interest.

References

Abboudi M, Messali M, Kadiri N, et al., 2011. Synthesis of CuO, La_2O_3, and La_2CuO_4 by the thermal-decomposition of oxalates precursors using a new method. *Synthesis and Reactivity in Inorganic, Metal-Organic, and Nano-Metal Chemistry*, 41(6):683-688. https://doi.org/10.1080/15533174.2011.568461

Balamurugan B, Mehta BR, Shivaprasad SM, 2001. Surface-modified CuO layer in size-stabilized single-phase Cu_2O nanoparticles. *Applied Physics Letters*, 79(19):3176-3178. https://doi.org/10.1063/1.1416478

Balasundaram K, Sharma M, 2018. Concurrent removal of elemental mercury and SO_2 from flue gas using a thiol-impregnated $CaCO_3$-based adsorbent: a full factorial design study. *Environmental Science and Pollution Research*, 25(16):15518-15528. https://doi.org/10.1007/s11356-018-1672-4

Bessinger BA, Vlassopoulos D, Serrano S, et al., 2012. Reactive transport modeling of subaqueous sediment caps and implications for the long-term fate of arsenic, mercury, and methylmercury. *Aquatic Geochemistry*, 18(4):297-326.

Blythe GM, Richardson MK, Dene CE, et al., 2010. Field study of mercury partitioning and re-emissions in wet FGD systems. Proceedings of the 8th Power Plant Air Pollutant Control Mega Symposium. https://doi.org/10.1007/s10498-012-9165-4

Bogacki J, Marcinowski P, Majewski M, et al., 2018. Alternative approach to current EU BAT recommendation for coal-fired power plant flue gas desulfurization wastewater treatment. *Processes*, 6(11):229. https://doi.org/10.3390/pr6110229

Bourne LC, Yu PY, Zettl A, et al., 1989. High-pressure electrical conductivity measurements in the copper oxides. *Physical Review B*, 40(16):10973-10976. https://doi.org/10.1103/PhysRevB.40.10973

Chakraborty S, Das A, Begum MR, et al., 2011. Vibrational properties of CuO nanoparticles synthesized by hydrothermal technique. *AIP Conference Proceedings*, 1349(1):841-842. https://doi.org/10.1063/1.3606120

Chang L, Zhao YC, Li HL, et al., 2017. Effect of sulfite on divalent mercury reduction and re-emission in a simulated desulfurization aqueous solution. *Fuel Processing Technology*, 165:138-144. https://doi.org/10.1016/j.fuproc.2017.05.016

Chen DY, Zhao SJ, Qu Z, et al., 2018. Cu-BTC as a novel material for elemental mercury removal from sintering gas. *Fuel*, 217:297-305. https://doi.org/10.1016/j.fuel.2017.12.086

Choi Y, Kim J, Moon I, 2020. Simulation and economic assessment of using H_2O_2 solution in wet scrubber for large marine vessels. *Energy*, 194:116907. https://doi.org/10.1016/j.energy.2020.116907

Devarajan D, Lian P, Brooks SC, et al., 2018. Quantum chemical approach for calculating stability constants of mercury complexes. *ACS Earth and Space Chemistry*, 2(11):1168-1178. https://doi.org/10.1021/acsearthspacechem.8b00102

Du W, Yin LB, Zhuo YQ, et al., 2015. Performance of CuO_x–neutral Al_2O_3 sorbents on mercury removal from simulated coal combustion flue gas. *Fuel Processing Technology*, 131:403-408. https://doi.org/10.1016/j.fuproc.2014.11.039

Fan XP, Li CT, Zeng GM, et al., 2012. The effects of Cu/HZSM-5 on combined removal of Hg^0 and NO from flue gas. *Fuel Processing Technology*, 104:325-331. https://doi.org/10.1016/j.fuproc.2012.06.003

Fang YR, Guo YB, 2018. Copper-based non-precious metal heterogeneous catalysts for environmental remediation. *Chinese Journal of Catalysis*, 39(4):566-582. https://doi.org/10.1016/S1872-2067(17)62996-6

Galloway B, Royko M, Sasmaz E, et al., 2018. Mercury oxidation over Cu-SSZ-13 catalysts under flue gas conditions. *Chemical Engineering Journal*, 336:253-262. https://doi.org/10.1016/j.cej.2017.11.163

Gao FY, Yan H, Tang XL, et al., 2021. Simultaneous removal of gaseous CO and elemental mercury over Cu-Co modified activated coke at low temperature. *Journal of Environmental Sciences*, 101:36-48. https://doi.org/10.1016/j.jes.2020.05.029

Gingerich DB, Grol E, Mauter MS, 2018. Fundamental challenges and engineering opportunities in flue gas desulfurization wastewater treatment at coal fired power plants. *Environmental Science: Water Research & Technology*, 4(7):909-925. https://doi.org/10.1039/c8ew00264a

He P, Zhang ZZ, Peng XL, et al., 2018. Mercury capture by manganese modified copper oxide. *Journal of the Taiwan Institute of Chemical Engineers*, 85:201-206. https://doi.org/10.1016/j.jtice.2018.01.045

Hsu CJ, Chiou HJ, Chen YH, et al., 2019. Mercury adsorption and re-emission inhibition from actual WFGD wastewater using sulfur-containing activated carbon. *Environmental Research*, 168:319-328. https://doi.org/10.1016/j.envres.2018.10.017

Hsu CJ, Atkinson JD, Chung A, et al., 2021. Gaseous mercury re-emission from wet flue gas desulfurization wastewater aeration basins: a review. *Journal of Hazardous Materials*, 420:126546. https://doi.org/10.1016/j.jhazmat.2021.126546

Jampaiah D, Chalkidis A, Sabri YM, et al., 2019. Role of ceria in the design of composite materials for elemental mercury removal. *The Chemical Record*, 19(7):1407-1419. https://doi.org/10.1002/tcr.201800161

Jia L, Fan BG, Yao YX, et al., 2018. Study on the elemental mercury adsorption characteristics and mechanism of iron-based modified biochar materials. *Energy & Fuels*, 32(12):12554-12566. https://doi.org/10.1021/acs.energyfuels.8b02890

Jiang XC, Herricks T, Xia YN, 2002. CuO nanowires can be synthesized by heating copper substrates in air. *Nano Letters*, 2(12):1333-1338. https://doi.org/10.1021/nl0257519

Lee J, Cho H, Moon I, et al., 2021. Techno-economic assessment of carbonate melt flue gas desulfurization process. *Computers & Chemical Engineering*, 146:107227. https://doi.org/10.1016/j.compchemeng.2021.107227

Lee J, Ahn Y, Cho H, et al., 2022. Economic performance assessment of elemental sulfur recovery with carbonate melt desulfurization process. *Process Safety and Environmental Protection*, 158:123-133. https://doi.org/10.1016/j.psep.2021.12.005

Li HL, Wu SK, Wu CY, et al., 2015. SCR atmosphere induced reduction of oxidized mercury over CuO–CeO_2/TiO_2 catalyst. *Environmental Science & Technology*, 49(12):7373-7379. https://doi.org/10.1021/acs.est.5b01104

Li HL, Zhu L, Wu SK, et al., 2017. Synergy of CuO and CeO_2 combination for mercury oxidation under low-temperature selective catalytic reduction atmosphere. *International Journal of Coal Geology*, 170:69-76. https://doi.org/10.1016/j.coal.2016.07.011

Li JY, Wu QR, Wang YY, et al., 2021. Improvement of NH_3 resistance over CuO/TiO_2 catalysts for elemental mercury oxidation in a wide temperature range. *Catalysis Today*, 376:276-284. https://doi.org/10.1016/j.cattod.2020.05.029

Li Y, Yang XY, Rooke J, et al., 2010. Ultralong $Cu(OH)_2$ and CuO nanowire bundles: PEG200-directed crystal growth for enhanced photocatalytic performance. *Journal of Colloid and Interface Science*, 348(2):303-312. https://doi.org/10.1016/j.jcis.2010.04.052

Lim J, Choi Y, Kim G, et al., 2020. Modeling of the wet flue gas desulfurization system to utilize low-grade limestone. *Korean Journal of Chemical Engineering*, 37(12):2085-2093. https://doi.org/10.1007/s11814-020-0639-6

Lim J, Cho H, Kim J, 2021. Optimization of wet flue gas desulfurization system using recycled waste oyster shell as high-grade limestone substitutes. *Journal of Cleaner Production*, 318:128492. https://doi.org/10.1016/j.jclepro.2021.128492

Lim J, Jeong S, Kim J, 2022. Deep neural network-based optimal selection and blending ratio of waste seashells as an alternative to high-grade limestone depletion for SO_x capture and utilization. *Chemical Engineering Journal*, 431:133244. https://doi.org/10.1016/j.cej.2021.133244

Liu DJ, Zhou WG, Wu J, 2017. Effect of Ce and La on the activity of CuO/ZSM-5 and MnO_x/ZSM-5 composites for elemental mercury removal at low temperature. *Fuel*, 194:115-122. https://doi.org/10.1016/j.fuel.2016.12.076

Liu DJ, Lu C, Wu J, 2018a. CuO/g-C_3N_4 nanocomposite for elemental mercury capture at low temperature. *Journal of Nanoparticle Research*, 20(10):277. https://doi.org/10.1007/s11051-018-4374-4

Liu DJ, Lu C, Wu J, 2018b. Gaseous mercury capture by copper-activated nanoporous carbon nitride. *Energy & Fuels*, 32(8):8287-8295. https://doi.org/10.1021/acs.energyfuels.8b01708

Liu DJ, Li CE, Wu J, et al., 2020. Novel carbon-based sorbents for elemental mercury removal from gas streams: a review. *Chemical Engineering Journal*, 391:123514. https://doi.org/10.1016/j.cej.2019.123514

Liu H, Chang L, Liu WJ, et al., 2020. Advances in mercury removal from coal-fired flue gas by mineral adsorbents. *Chemical Engineering Journal*, 379:122263. https://doi.org/10.1016/j.cej.2019.122263

Liu JP, Huang XT, Li YY, et al., 2006. Hierarchical nanostructures of cupric oxide on a copper substrate: controllable morphology and wettability. *Journal of Materials Chemistry*, 16(45):4427-4434. https://doi.org/10.1039/b611691d

Liu Z, Liu DY, Zhao BT, et al., 2020. Mercury removal based on adsorption and oxidation by fly ash: a review. *Energy & Fuels*, 34(10):11840-11866. https://doi.org/10.1021/acs.energyfuels.0c02209

Liu ZL, Wang DL, Peng B, et al., 2017. Mercury re-emission in the smelting flue gas cleaning process: the influence of arsenite. *Energy & Fuels*, 31(10):11053-11059. https://doi.org/10.1021/acs.energyfuels.7b01733

Long YF, He Z, Li XY, et al., 2022. Removal of elemental mercury from flue gas using the magnetic attapulgite by Mn-Cu oxides modification. *Environmental Science and Pollution Research*, 29(10):14058-14069. https://doi.org/10.1007/s11356-021-16777-z

Ma YP, Xu HM, Qu Z, et al., 2014. Absorption characteristics of elemental mercury in mercury chloride solutions. *Journal of Environmental Sciences*, 26(11):2257-2265. https://doi.org/10.1016/j.jes.2014.09.011

Ma YP, Xu TF, Li L, et al., 2021. Core-shell nanostructure α-Fe_2O_3/SnO_2 binary oxides for the catalytic oxidation and adsorption of elemental mercury from flue gas. *Journal of Environmental Chemical Engineering*, 9(2):105137. https://doi.org/10.1016/j.jece.2021.105137

Mei J, Wang C, Kong LN, et al., 2019. Outstanding performance of recyclable amorphous MoS_3 supported on TiO_2 for capturing high concentrations of gaseous elemental mercury: mechanism, kinetics, and application. *Environmental Science & Technology*, 53(8):4480-4489. https://doi.org/10.1021/acs.est.9b00464

Mei J, Wang C, Kong LN, et al., 2020. Remarkable improvement of Ti incorporation on Hg^0 capture from smelting flue gas by sulfurated γ-Fe_2O_3: performance and mechanism. *Journal of Hazardous Materials*, 381:120967.

https://doi.org/10.1016/j.jhazmat.2019.120967

Mei ZJ, Shen ZM, Zhao QJ, et al., 2008. Removing and recovering gas-phase elemental mercury by $Cu_xCo_{3-x}O_4$ ($0.75\leqslant x\leqslant 2.25$) in the presence of sulphur compounds. *Chemosphere*, 70(8):1399-1404. https://doi.org/10.1016/j.chemosphere.2007.09.024

Neupane MP, Kim YK, Park IS, et al., 2009. Temperature driven morphological changes of hydrothermally prepared copper oxide nanoparticles. *Surface and Interface Analysis*, 41(3):259-263. https://doi.org/10.1002/sia.3009

Omine N, Romero CE, Kikkawa H, et al., 2012. Study of elemental mercury re-emission in a simulated wet scrubber. *Fuel*, 91(1):93-101. https://doi.org/10.1016/j.fuel.2011.06.018

Peng B, Liu ZL, Chai LY, et al., 2016. The effect of selenite on mercury re-emission in smelting flue gas scrubbing system. *Fuel*, 168:7-13. https://doi.org/10.1016/j.fuel.2015.11.072

Poizot P, Hung CJ, Nikiforov MP, et al., 2003. An electrochemical method for CuO thin film deposition from aqueous solution. *Electrochemical and Solid-State Letters*, 6(2):C21-C25. https://doi.org/10.1149/1.1535753

Powell KJ, Brown PL, Byrne RH, et al., 2005. Chemical speciation of environmentally significant heavy metals with inorganic ligands. Part 1: the Hg^{2+}–Cl^-, OH^-, CO_3^{2-}, SO_4^{2-}, and PO_4^{3-} aqueous systems (IUPAC technical report). *Pure and Applied Chemistry*, 77(4):739-800. https://doi.org/10.1351/pac200577040739

Radhakrishnan A, Rejani P, Beena B, 2014. Synthesis, characterization and antimicrobial properties of CuO nanoparticles against gram-positive and gram-negative bacterial strains. *International Journal of Nano Dimension*, 5(6): 519-524.

Sun PX, Mei J, Wang C, et al., 2021. Outstanding performance of CuO/Fe-Ti spinel for Hg^0 oxidation as a co-benefit of no abatement: significant promotion of Hg^0 oxidation by CuO loading. *Catalysis Science & Technology*, 11(6):2316-2326. https://doi.org/10.1039/d0cy02081h

Tang L, Li CT, Zhao LK, et al., 2018. A novel catalyst CuO-ZrO_2 doped on Cl^- activated bio-char for Hg^0 removal in a broad temperature range. *Fuel*, 218:366-374. https://doi.org/10.1016/j.fuel.2018.01.051

Toboonsung B, Singjai P, 2011. Formation of CuO nanorods and their bundles by an electrochemical dissolution and deposition process. *Journal of Alloys and Compounds*, 509(10):4132-4137. https://doi.org/10.1016/j.jallcom.2010.12.180

Ulyankina A, Leontyev I, Maslova O, et al., 2018. Copper oxides for energy storage application: novel pulse alternating current synthesis. *Materials Science in Semiconductor Processing*, 73:111-116. https://doi.org/10.1016/j.mssp.2017.08.001

van Loon LL, Mader EA, Scott SL, 2001. Sulfite stabilization and reduction of the aqueous mercuric ion: kinetic determination of sequential formation constants. *The Journal of Physical Chemistry A*, 105(13):3190-3195. https://doi.org/10.1021/jp003803h

Vidyasagar CC, Naik YA, Venkatesha TG, et al., 2012. Solid-state synthesis and effect of temperature on optical properties of CuO nanoparticles. *Nano-Micro Letters*, 4(2): 73-77. https://doi.org/10.1007/BF03353695

Wang C, Zhang XF, Mei J, et al., 2020. Outstanding performance of magnetically separable sulfureted MoO_3/Fe-Ti spinel for gaseous Hg^0 recovery from smelting flue gas: mechanism and adsorption kinetics. *Environmental Science & Technology*, 54(12):7659-7668. https://doi.org/10.1021/acs.est.0c01373

Wang HN, Ma W, Yan JB, et al., 2020. Smart modification of HZSM-5 with manganese species for the removal of mercury. *ACS Omega*, 5(30):19277-19284. https://doi.org/10.1021/acsomega.0c02877

Wang HY, Wang BD, Zhou JL, et al., 2019. CuO modified vanadium-based SCR catalysts for Hg^0 oxidation and NO reduction. *Journal of Environmental Management*, 239: 17-22. https://doi.org/10.1016/j.jenvman.2019.02.118

Wang J, Kong X, Du R, et al., 2012. Removal of vapor-phase elemental mercury over a CuO/AC catalyst. The 2nd International Conference on Energy, Environment and Sustainable Development (EESD 2012), p.64-67.

Wang PY, Su S, Xiang J, et al., 2013. Catalytic oxidation of Hg^0 by CuO-MnO_2-Fe_2O_3/γ-Al_2O_3 catalyst. *Chemical Engineering Journal*, 225:68-75. https://doi.org/10.1016/j.cej.2013.03.060

Wang Y, Si WZ, Peng Y, et al., 2019. Investigation on removal of NO and Hg^0 with different Cu species in Cu-SAPO-34 zeolites. *Catalysis Communications*, 119:91-95. https://doi.org/10.1016/j.catcom.2018.10.019

Wang Z, Liu J, Yang YJ, et al., 2020. AMn_2O_4 (A=Cu, Ni and Zn) sorbents coupling high adsorption and regeneration performance for elemental mercury removal from syngas. *Journal of Hazardous Materials*, 388:121738. https://doi.org/10.1016/j.jhazmat.2019.121738

Wen XY, Li CT, Fan XP, et al., 2011. Experimental study of gaseous elemental mercury removal with CeO_2/γ-Al_2O_3. *Energy & Fuels*, 25(7):2939-2944. https://doi.org/10.1021/ef200144j

Xiang WJ, Liu J, Chang M, et al., 2012. The adsorption mechanism of elemental mercury on CuO (1 1 0) surface. *Chemical Engineering Journal*, 200-202:91-96. https://doi.org/10.1016/j.cej.2012.06.025

Xu JF, Ji W, Shen ZX, et al., 1999. Preparation and characterization of CuO nanocrystals. *Journal of Solid State Chemistry*, 147(2):516-519. https://doi.org/10.1006/jssc.1999.8409

Xu W, Adewuyi YG, Liu YX, et al., 2018. Removal of elemental mercury from flue gas using CuO_x and CeO_2 modified rice straw chars enhanced by ultrasound. *Fuel Processing Technology*, 170:21-31. https://doi.org/10.1016/j.fuproc.2017.10.017

Xu WQ, Wang HR, Zhou X, et al., 2014. CuO/TiO_2 catalysts for gas-phase Hg^0 catalytic oxidation. *Chemical Engineering Journal*, 243:380-385. https://doi.org/10.1016/j.cej.2013.12.014

Yang C, Su XT, Wang JD, et al., 2013. Facile microwave-assisted hydrothermal synthesis of varied-shaped CuO

nanoparticles and their gas sensing properties. *Sensors and Actuators B: Chemical*, 185:159-165. https://doi.org/10.1016/j.snb.2013.04.100

Yang JP, Zhao YC, Zhang JY, et al., 2014. Regenerable cobalt oxide loaded magnetosphere catalyst from fly ash for mercury removal in coal combustion flue gas. *Environmental Science & Technology*, 48(24):14837-14843. https://doi.org/10.1021/es504419v

Yang R, Mei CL, Wu XS, et al., 2019. Mn-Cu binary metal oxides with molecular-scale homogeneity for Hg^0 removal from coal-fired flue gas. *Industrial & Engineering Chemistry Research*, 58(41):19292-19301. https://doi.org/10.1021/acs.iecr.9b04005

Yang SJ, Guo YF, Yan NQ, et al., 2011a. Elemental mercury capture from flue gas by magnetic Mn-Fe spinel: effect of chemical heterogeneity. *Industrial & Engineering Chemistry Research*, 50(16):9650-9656. https://doi.org/10.1021/ie2009873

Yang SJ, Guo YF, Yan NQ, et al., 2011b. Nanosized cation-deficient Fe-Ti spinel: a novel magnetic sorbent for elemental mercury capture from flue gas. *ACS Applied Materials & Interfaces*, 3(2):209-217. https://doi.org/10.1021/am100835c

Yang W, Liu YX, Wang Q, et al., 2017. Removal of elemental mercury from flue gas using wheat straw chars modified by Mn-Ce mixed oxides with ultrasonic-assisted impregnation. *Chemical Engineering Journal*, 326:169-181. https://doi.org/10.1016/j.cej.2017.05.106

Yang W, Li Y, Shi S, et al., 2019. Mercury removal from flue gas by magnetic iron-copper oxide modified porous char derived from biomass materials. *Fuel*, 256:115977. https://doi.org/10.1016/j.fuel.2019.115977

Yang YJ, Liu J, Zhang BK, et al., 2017. Experimental and theoretical studies of mercury oxidation over CeO_2-WO_3/TiO_2 catalysts in coal-fired flue gas. *Chemical Engineering Journal*, 317:758-765. https://doi.org/10.1016/j.cej.2017.02.060

Yang YJ, Miao S, Liu J, et al., 2019a. Cost-effective manganese ore sorbent for elemental mercury removal from flue gas. *Environmental Science & Technology*, 53(16):9957-9965. https://doi.org/10.1021/acs.est.9b03397

Yang YJ, Liu J, Wang Z, et al., 2019b. Interface reaction activity of recyclable and regenerable Cu-Mn spinel-type sorbent for Hg^0 capture from flue gas. *Chemical Engineering Journal*, 372:697-707. https://doi.org/10.1016/j.cej.2019.04.177

Yang YJ, Liu J, Wang Z, et al., 2019c. Nature of active sites and an oxygen-assisted reaction mechanism for mercury capture by spinel-type $CuMn_2O_4$ sorbents. *Energy & Fuels*, 33(9):8920-8926. https://doi.org/10.1021/acs.energyfuels.9b01696

Yang YJ, Liu J, Ding JY, et al., 2022. Mercury/oxygen reaction mechanism over $CuFe_2O_4$ catalyst. *Journal of Hazardous Materials*, 424:127556. https://doi.org/10.1016/j.jhazmat.2021.127556

Ye D, Wang XX, Wang RX, et al., 2021. Recent advances in MnO_2-based adsorbents for mercury removal from coal-fired flue gas. *Journal of Environmental Chemical Engineering*, 9(5):105993. https://doi.org/10.1016/j.jece.2021.105993

Yi YY, Li CT, Zhao LK, et al., 2018. The synthetic evaluation of CuO-MnO_x-modified pinecone biochar for simultaneous removal formaldehyde and elemental mercury from simulated flue gas. *Environmental Science and Pollution Research*, 25(5):4761-4775. https://doi.org/10.1007/s11356-017-0855-8

Yuan GQ, Jiang HF, Lin C, et al., 2007. Shape- and size-controlled electrochemical synthesis of cupric oxide nanocrystals. *Journal of Crystal Growth*, 303(2):400-406. https://doi.org/10.1016/j.jcrysgro.2006.12.047

Yue HF, Lu P, Su W, et al., 2019. Simultaneous removal of NO_x and Hg^0 from simulated flue gas over $Cu_aCe_bZr_cO_3$/r-Al_2O_3 catalysts at low temperatures: performance, characterization, and mechanism. *Environmental Science and Pollution Research*, 26(13):13602-13618. https://doi.org/10.1007/s11356-019-04822-x

Zhang HC, Wang T, Liu J, et al., 2020. Promotional effect of sulfur trioxide (SO_3) on elemental mercury removal over Cu/ZSM-5 catalyst. *Applied Surface Science*, 511:145604. https://doi.org/10.1016/j.apsusc.2020.145604

Zhang J, Duan YF, Zhao WX, et al., 2016. Removal of elemental mercury from simulated flue gas by combining non-thermal plasma with calcium oxide. *Plasma Chemistry and Plasma Processing*, 36(2):471-485. https://doi.org/10.1007/s11090-015-9668-z

Zhang Q, Mei J, Sun PX, et al., 2020. Mechanism of elemental mercury oxidation over copper-based oxide catalysts: kinetics and transient reaction studies. *Industrial & Engineering Chemistry Research*, 59(1):61-70. https://doi.org/10.1021/acs.iecr.9b04806

Zhang X, Guo YG, Liu WM, et al., 2008. CuO three-dimensional flowerlike nanostructures: controlled synthesis and characterization. *Journal of Applied Physics*, 103(11):114304. https://doi.org/10.1063/1.2939237

Zhang XY, Cui L, Li YZ, et al., 2019. Adsorption and oxidation of mercury by montmorillonite powder modified with different copper compounds. *Energy & Fuels*, 33(8):7852-7860. https://doi.org/10.1021/acs.energyfuels.9b01294

Zhang Z, Liu J, Wang Z, et al., 2021a. Bimetallic Fe-Cu-based metal-organic frameworks as efficient adsorbents for gaseous elemental mercury removal. *Industrial & Engineering Chemistry Research*, 60(1):781-789. https://doi.org/10.1021/acs.iecr.0c04298

Zhang Z, Liu J, Wang Z, et al., 2021b. Efficient capture of gaseous elemental mercury based on novel copper-based metal-organic frameworks. *Fuel*, 289:119791. https://doi.org/10.1016/j.fuel.2020.119791

Zhao B, Yi HH, Tang XL, et al., 2019. Using CuO-MnO_x/AC-H as catalyst for simultaneous removal of Hg^0 and NO from coal-fired flue gas. *Journal of Hazardous Materials*, 364:700-709. https://doi.org/10.1016/j.jhazmat.2018.04.001

Zhao LL, Huang Y, Chen HY, et al., 2017. Study on the preparation of bimetallic oxide sorbent for mercury removal. *Fuel*, 197:20-27. https://doi.org/10.1016/j.fuel.2017.01.122

Zheng W, Li HL, Yang ZQ, et al., 2021. Advances in flue gas mercury abatement by mineral chalcogenides. *Chemical Engineering Journal*, 411:128608. https://doi.org/10.1016/j.cej.2021.128608